Single-nucleon transfer reactions induced by ^{11}B ions on ^{208}Pb: A test of the distorted-wave Born approximation

J. L. C. Ford, Jr., K. S. Toth, G. R. Satchler, D. C. Hensley, and L. W. Owen
Oak Ridge National Laboratory, Oak Ridge, Tennessee 37830*

R. M. DeVries†
University of Washington, Seattle, Washington 98105

R. M. Gaedke‡
Trinity University, San Antonio, Texas 78212

P. J. Riley‡
University of Texas, Austin, Texas 78712

S. T. Thornton‡
University of Virginia, Charlottesville, Virginia 22903
(Received 10 April 1974)

A 100-$\mu g/cm^2$ thick ^{208}Pb target was bombarded with 72.2-MeV ^{11}B ions accelerated in the Oak Ridge isochronous cyclotron. Reaction products were detected at the focal plane of an Elbek spectrograph using a 60-cm long position-sensitive proportional counter. In addition to determining the position of the detected particle along the focal plane, the energy loss in the counter helped to identify the particle type. Angular distributions were measured for all four possible single-nucleon transfer reaction products, i.e., ^{10}Be, ^{10}B, ^{12}C, and ^{12}B. These reactions were found to excite single-particle or single-hole states in the heavy residual nuclei, though some groups corresponding to the light ions being left in excited states were also identified. A finite-range distorted-wave Born-approximation analysis including exactly the effects due to recoil was made of these differential cross sections with particular attention being paid to various uncertainties. The major uncertainties arise from the choice of potentials (especially in the exit channels) and of form factors for the bound nucleon before and after transfer. Except for the (^{11}B, ^{10}B) reactions, which suffer from an unfavorable matching between incoming and outgoing orbits, the predicted angular distributions were in good agreement with the data, with extracted spectroscopic factors close to expected values and to those obtained in other light- and heavy-ion experiments. The indication then is that these reactions are predominantly one-step processes, though there is some evidence of the need for other effects to be considered.

[NUCLEAR REACTIONS $^{208}Pb(^{11}B, ^{10}B)$, $^{208}Pb(^{11}B, ^{12}B)$, $^{208}Pb(^{11}B, ^{10}Be)$, $^{208}Pb(^{11}B, ^{12}C)$, $E_L = 72.2$ MeV; measured $\sigma(\theta)$; optical model and DWBA analyses; deduced spectroscopic factors. Enriched target.]

I. INTRODUCTION

A more complete understanding of heavy-ion single-nucleon transfer reactions is not only necessary in order to extract reliable spectroscopic information from such reactions, but also to form the basis for understanding more complicated heavy-ion reactions. A favorable case for studying the reaction mechanism is one involving a closed shell target nucleus in which single-particle and single-hole states are strongly excited.[1-9] A good target for this is ^{208}Pb.

In addition, single-nucleon transfer with heavy ions is a useful spectroscopic tool in itself just because it picks out the single particle and hole components in the states it excites. The strong Q dependence of these reactions often permits the reaction and incident energy to be chosen so as to preferentially select the states of greatest interest, including cases where single-nucleon transfer reactions with light ions have small cross sections due to Q value dependence. In addition, two-step and other indirect processes may be important in single-nucleon transfer with heavy ions permitting the excitation of states not easily accessible with light-ion reactions.[10] Consequently, it is of considerable interest to have a detailed comparison between measurements and the predictions of the distorted-wave Born approximation (DWBA).

Single-nucleon heavy-ion transfer reactions are dominated by kinematic effects below the Coulomb barrier (see, e.g., Ref. 11). At energies well above the barrier kinematic effects may still be important, but one still expects the reaction mech-

anism to be direct and perhaps interpretable in terms of a DWBA analysis. Measurements involving single-nucleon transfer with ^{12}C ions,[1] ^{11}B ions,[2,3] and ^{16}O ions[4] on ^{208}Pb at energies above the Coulomb barrier gave angular distributions which were structureless and single-peaked at the angle corresponding to the classical Rutherford orbit for grazing collisions. Despite this classical nature of single-nucleon transfer reactions systematic differences have been observed between neutron pickup and proton stripping with heavy ions. For the case of ^{12}C ions incident on ^{208}Pb, the peak angles for neutron pickup shifted to higher values with increasing excitation energy in the residual nucleus in contrast to single proton stripping where the peak angle remained constant.[1] This effect, as well as the possible j and L dependence of heavy-ion reactions which has been observed in (^{12}C, ^{11}B), (^{14}N, ^{13}C), and (^{16}O, ^{15}N) reactions,[4-6] have now been reproduced by exact finite-range distorted-wave calculations which include recoil effects, although sometimes it has required the arbitrary adjustment of optical potentials in the exit channel.[12-14]

We report here an investigation of single neutron and proton stripping and pickup by means of $^{11}B + ^{208}Pb$ reactions at an incident energy of 72.2 MeV. All four single-nucleon transfer reactions (^{11}B, ^{10}B), (^{11}B, ^{12}B), (^{11}B, ^{10}Be), and (^{11}B, ^{12}C) were observed, and angular distributions for final states in ^{209}Pb, ^{207}Pb, ^{209}Bi, and ^{207}Tl were measured, as well as for some particle groups corresponding to excitation of the outgoing light reaction product. An exact finite-range DWBA analysis (thus including effects due to recoil[12]) has been made, and is discussed along with the extracted spectroscopic factors in Secs. VI and VII.

II. EXPERIMENTAL PROCEDURE

The large number of reaction products possible in heavy-ion reactions requires that the detection system have both good energy and mass resolution for spectroscopic studies. Magnetic spectrometers provide good momentum resolution as well as kinematic compensation for the large energy variation with angle for particles emitted in heavy-ion interactions. Thus, when used with active focal plane detectors magnetic spectrometers are well suited to study heavy-ion-induced reactions. In addition to determining the position along the focal plane, position-sensitive detectors provide supplementary information, such as the energy lost in the detector, to help distinguish the particle type.[15,16]

In the present experiment the reaction products were detected at the focal plane of an Elbek spectrograph by using a 60-cm long position-sensitive proportional counter of the Borkowski-Kopp design.[17,18] The detector, shown schematically in Fig. 1, has three 0.0076-cm diam high-resistivity pyrolytic-coated quartz wires spaced over a vertical height of 5.03 cm in order to match the image spot at the focal plane, and thus utilize the full solid angle of the magnet. The 0.0013-cm Mylar foil shown in the figure maintained the pressure difference between the counter gas volume and the high vacuum of the spectrometer camera box while the inner 0.0038-cm aluminized Mylar foil defined the field region above the detector. The depth of the field region, 0.5 cm, and the counter pressure of about one-third of an atmosphere (90% argon-

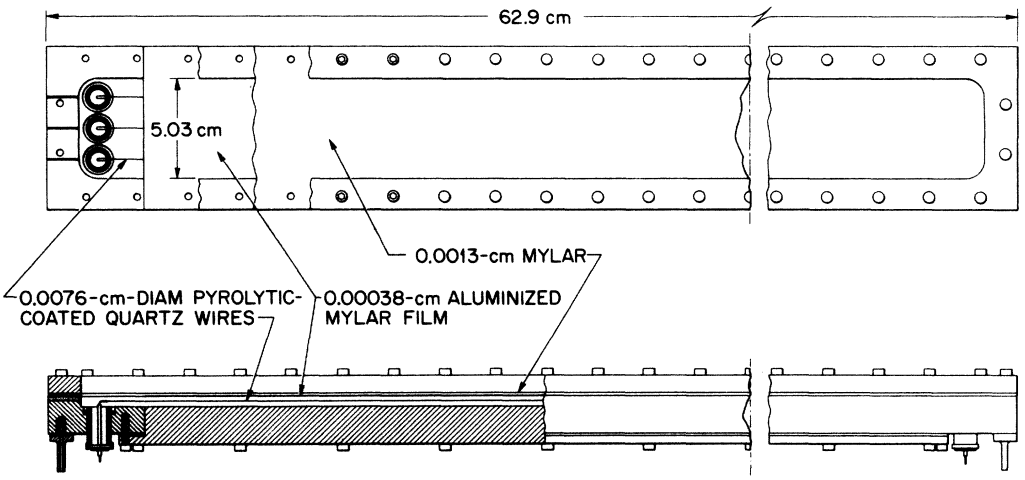

FIG. 1. Assembly drawing of the three-wire, 60-cm long proportional detector.

10% methane) resulted in an energy loss of ~0.5 MeV for 72-MeV ^{11}B ions, and a ΔE resolution varying from about 10 to 14% for the different ions detected.

The electronic system used with the detector is shown in Fig. 2. A total of four preamplifiers was used with the network of three wires in the manner described by Borkowski and Kopp.[18] The signals obtained by summing the two preamplifiers at the left end of the detector and the two preamplifiers at the right end of the detector provided timing signals which determined the position of the detected particle x along the focal plane. However, the response of the three wires is sufficiently different so that the resolution of the system is spoiled if the position signals of the wires are simply added. To avoid this the response of the two preamplifiers at the top and bottom of the network shown in Fig. 2 are also added, and the time difference between these two signals served to identify which of the three wires y was involved. The separate response of each wire was calibrated by using a ^{244}Cm α particle source and by shifting the elastic ^{11}B peak along the detector. The signal from each wire was then adjusted during the experiment by using a computer program before it was added to the total spectrum of the three wires.

The sum of all four preamplifiers was also amplified, using a long-time constant to fully integrate the collected charge, to furnish a signal proportional to the energy lost in the counter by the detected particle. This ΔE signal served to identify the particle type. The Q value, or position along the focal plane, also helped to separate the various particle groups.

The three pieces of information provided by the detector, i.e., ΔE, position x, and wire-identification signal y, were digitized with an an analog-to-digital-converter (ADC) system which has approximately a 9000-channel resolution capability and is interfaced to an in-house computer. The experimental data were stored in this computer in a two-dimensional (ΔE by x) mode. Pulse height spectra of the particle types of interest could then be generated as needed from this two-dimensional array.

The 72.2-MeV ^{11}B beam from the Oak Ridge isochronous cyclotron was used to bombard a 100-μg/cm^2 thick ^{208}Pb target evaporated onto a 40-μg/cm^2 thick carbon foil. Because the beam current was limited to 200 nA to avoid breaking the target foil, data were accumulated at each angle for about four hours to obtain reasonable counting statistics.

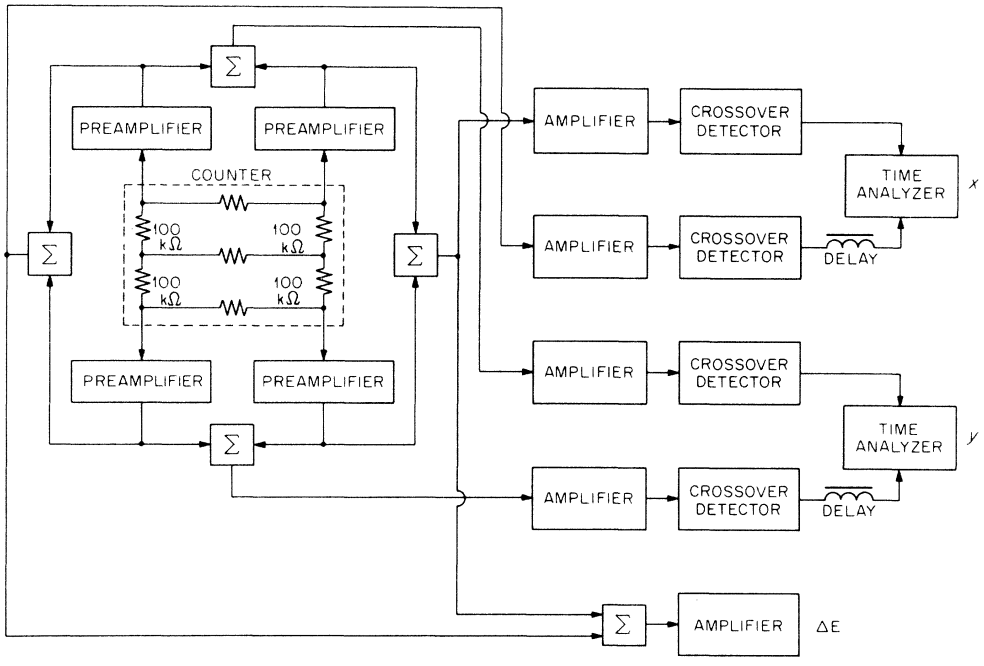

FIG. 2. Schematic of detector and associated electronic system. The middle high-resistivity wire is separated at each of its ends from the two outside wires by 100-kΩ resistors. The three signals from the system are identified as: x, the position along the focal plane; y, the signal specifying from which of the three wires the x signal originates; and ΔE, the energy lost in the counter by the detected particle.

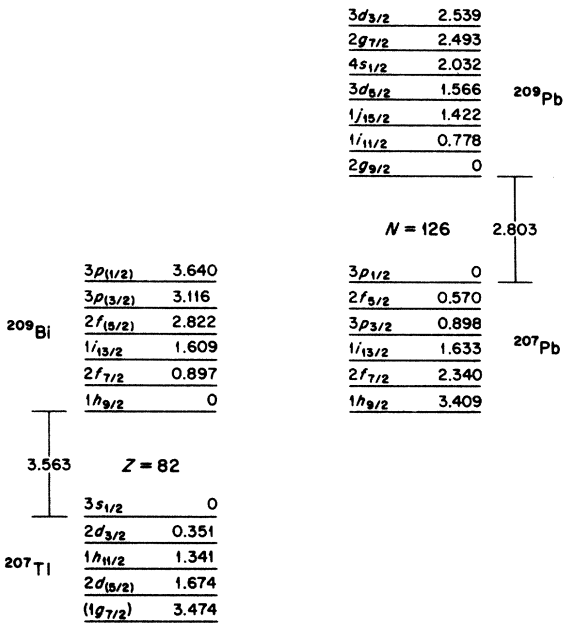

FIG. 3. A summary of the shell-model orbits in the ^{208}Pb mass region taken from Ref. 19.

III. EXPERIMENTAL RESULTS

The single-particle and single-hole states which could be excited in these reactions are summarized[19] in Fig. 3. The high energy portion of the energy spectra for the neutron pickup and stripping reactions ^{208}Pb(^{11}B, ^{12}B)^{207}Pb and ^{208}Pb(^{11}B, ^{10}B)^{209}Pb are shown in Fig. 4 for a laboratory angle of 55°. The proton pickup and stripping reactions ^{208}Pb(^{11}B, ^{12}C)^{207}Tl and ^{208}Pb(^{11}B, ^{10}Be)^{209}Bi are shown in Figs. 5 and 6 for laboratory angles of 52.5 and 47.5°, respectively. The energy resolution typically ranged from about 185 to 250 keV, and was limited by the target thickness and incident beam resolution rather than by the magnet or detector. Magnetic field settings could be selected so that ^{10}B, ^{11}B, ^{12}B, and ^{12}C particles were detected simultaneously by the counter. Different settings, however, had to be used to observe ^{10}Be particles due to their much larger momentum. At these settings only the high energy portions of the ^{11}B and ^{12}B particles were recorded while the ^{10}Be spectrum extended over almost the whole length of the detector.

All four reactions predominately populated known (see Fig. 3) single particle or hole states. The (^{11}B, ^{12}B) reaction shown in Fig. 4 populated the $3p_{1/2}{}^{-1}$, $2f_{5/2}{}^{-1}$, $3p_{3/2}{}^{-1}$, and $2f_{7/2}{}^{-1}$ hole states in ^{207}Pb.

The $1i_{13/2}{}^{-1}$ state at 1.64 MeV lies under the intense peak due to elastic scattered ^{11}B particles. The $2g_{9/2}$, $1i_{11/2}$, $1j_{15/2}$, $3d_{5/2}$, and $2g_{7/2}$ states in ^{209}Pb were observed in the (^{11}B, ^{10}B) reaction. We were unable to observe the $3d_{3/2}$ state known to be at 2.54 MeV (see Fig. 3) and estimate its contribution to the $2g_{7/2}$ state to be less than 10%. Also, as we shall see below, the small peak near 2.1 MeV is more likely due to emission of ^{10}B in an excited state rather than being due to its feeding the

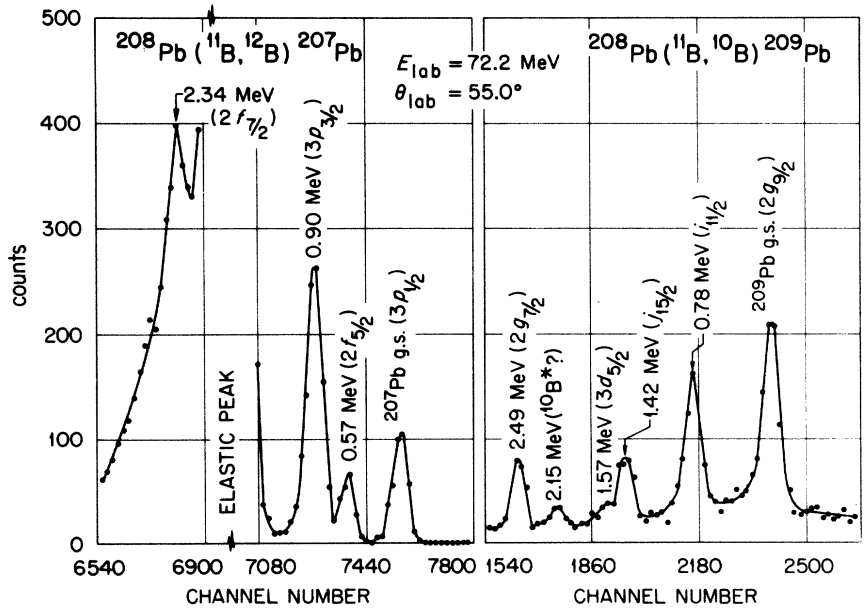

FIG. 4. Energy spectra measured at 55° (lab) and an incident energy of 72.2 MeV for the (^{11}B, ^{12}B) and (^{11}B, ^{10}B) reactions on ^{208}Pb leading to states in ^{207}Pb and ^{209}Pb, respectively.

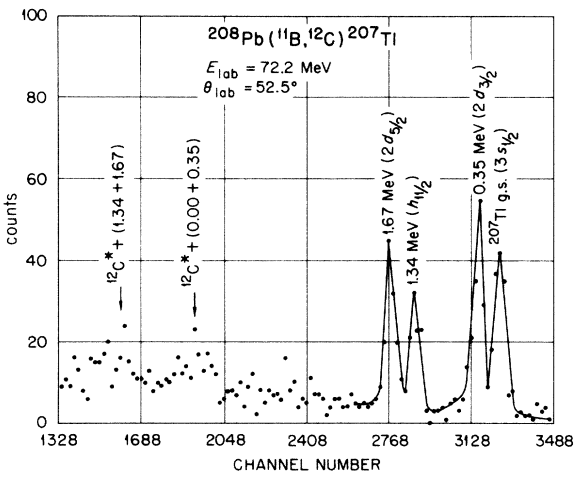

FIG. 5. An energy spectrum measured at 52.5° (lab) and an incident energy of 72.2 MeV for the (^{11}B, ^{12}C) reaction on ^{208}Pb leading to states in ^{207}Tl.

$4s_{1/2}$ state at 2.03 MeV in ^{209}Pb.

The (^{11}B, ^{12}C) reaction shown in Fig. 5 strongly populates the $3s_{1/2}^{-1}$, $2d_{3/2}^{-1}$, $1h_{11/2}^{-1}$, and $3d_{5/2}^{-1}$ states in ^{207}Tl. There are also peaks that correspond to these same groups accompanied by the emission of ^{12}C in its 2^+ excited state at 4.43 MeV. The single particle states observed in the (^{11}B, ^{10}Be) spectrum are as follows: $1h_{9/2}$, $2f_{7/2}$, $1i_{13/2}$, $2f_{5/2}$, $3p_{3/2}$, and $3p_{1/2}$. We might add that these $3p$ states were not seen in the measurements of Anyas-Weiss *et al.*[3] at 113.5-MeV ^{11}B bombarding energy. Intense peaks are seen in Fig. 6 at energies consistent with the emission of the ^{10}Be nucleus in its first 2^+ level at 3.37 MeV along with transitions to states in ^{209}Bi. The remainder of the ^{10}Be spectrum extended up to ~20 MeV in excitation and was free of contamination from other particle groups except at an energy region corresponding to where the intense ^{11}B elastic peak was located. There was no evidence for the breakup of the incident ^{11}B ions into ^{10}Be and a proton by the Coulomb field of the target.

Angular distributions for the strong states observed are shown in Figs. 7 through 12. Experimental uncertainties indicated in the figures represent only statistical errors. The curves in Figs. 7–12 are the calculated DWBA results discussed in Sec. VII.

IV. KINEMATIC EFFECTS

Reactions for which the value of the Sommerfield parameter $n = Z_1 Z_2 e^2/\hbar v$, is large can be expected to be reasonably well described by semiclassical models.[20,21] In the present experiment the values of n varied from 20 to 30 depending on the reaction involved and the final state populated. The single-peaked and smooth angular distributions observed can also be interpreted in terms of well-known semiclassical concepts. The peaks of these angular distributions occur at angles close to the classical grazing angle.

Heavy-ion reactions often exhibit a strong dependence on the Q value due to the need to match the incoming and outgoing orbits at the nuclear surface. For energies above the Coulomb barrier the most appropriate expression for the optimum Q value for a reaction $A(a, b)B$ is probably that given

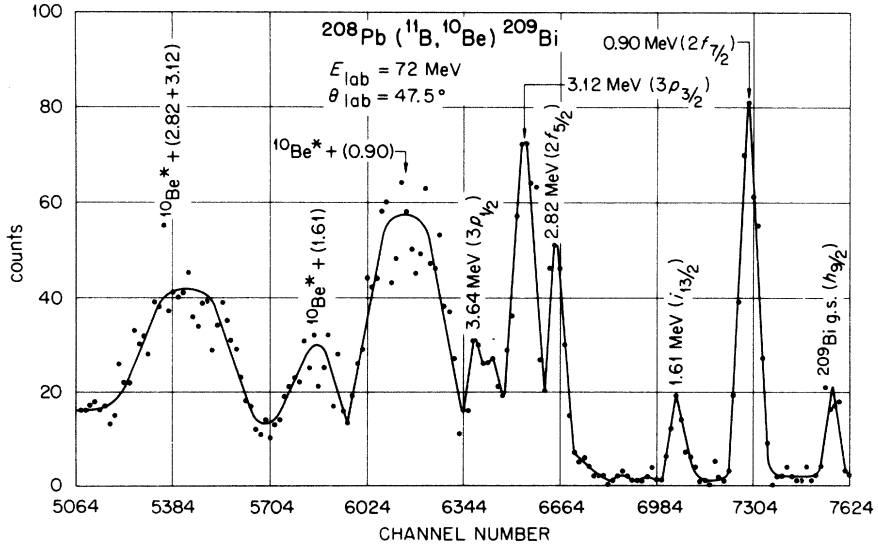

FIG. 6. An energy spectrum measured at 47.5° (lab) and at an incident energy of 72.2 MeV for the (^{11}B, ^{10}Be) reaction on ^{208}Pb leading to states in ^{209}Bi.

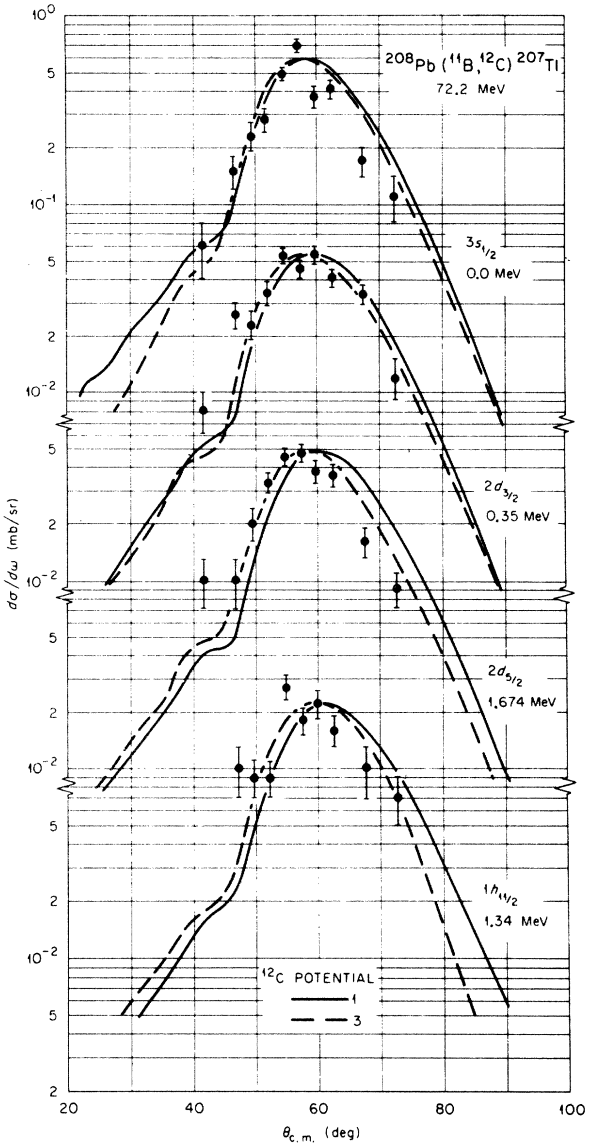

FIG. 7. Differential cross sections for groups from the (^{11}B, ^{12}C) reactions. The curves are DWBA calculations normalized with the spectroscopic factors in Table V. Two different potentials were used for the ^{12}C exit channel (see Table I).

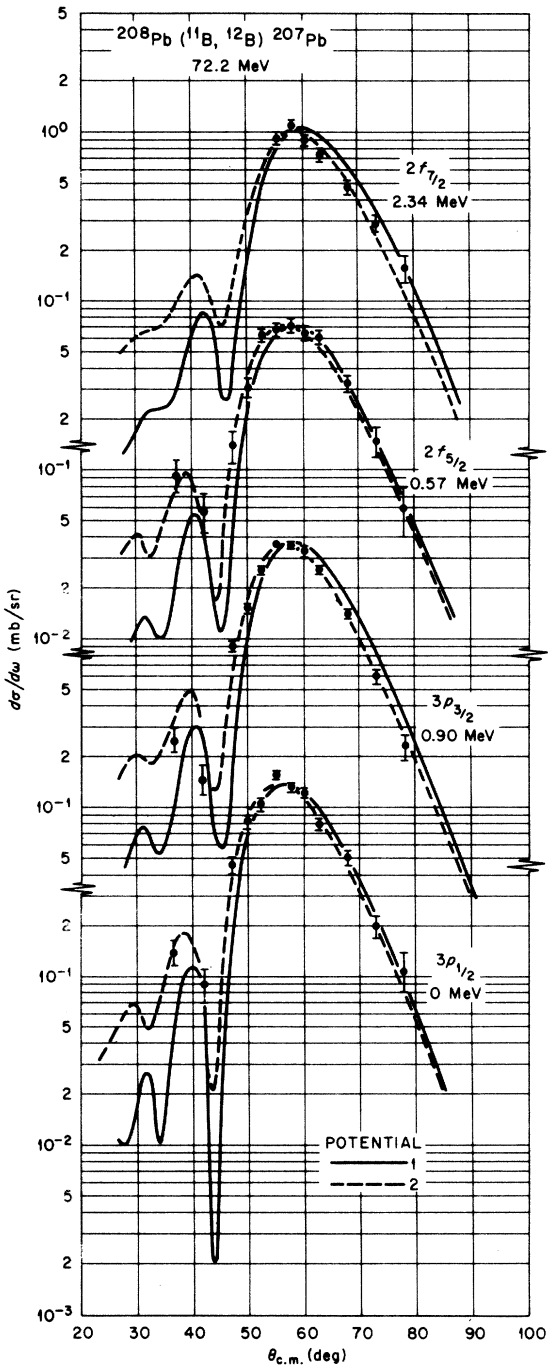

FIG. 8. Differential cross sections for groups from the (^{11}B, ^{12}B) reactions. The curves are DWBA calculations normalized with the spectroscopic factors in Table VI. Either potential 1 or 2 (see Table I) was used in both entrance and exit channels.

by Brink,[3,22]

$$Q_{\text{opt}} = (Z_b Z_B - Z_a Z_A) e^2/R - \tfrac{1}{2} m v^2 , \qquad (1)$$

where $Z_i e$ is the charge on nucleus i, v is the relative velocity of the two nuclei in the region of interaction where they are separated by R, and m is the mass of the transferred particle. The optimum angular momentum transfer is given by the difference in angular momenta of the incoming and outgoing orbits, i.e., those whose distance of closest approach is R,

$$L_{\text{opt}} = |L_a - L_b| . \qquad (2)$$

We may take the strong absorption radius for R

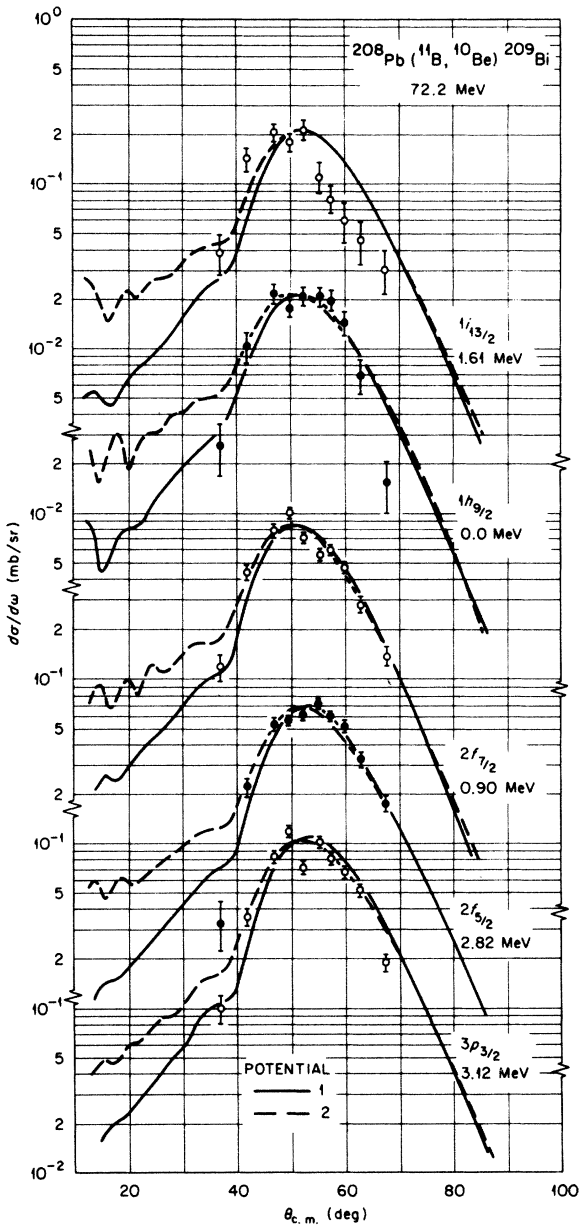

FIG. 9. Differential cross sections for groups from the (^{11}B, ^{10}Be) reactions. The curves are DWBA calculations normalized with the spectroscopic factors in Table VII. Either potential 1 or 2 (see Table I) was used in both entrance and exit channels.

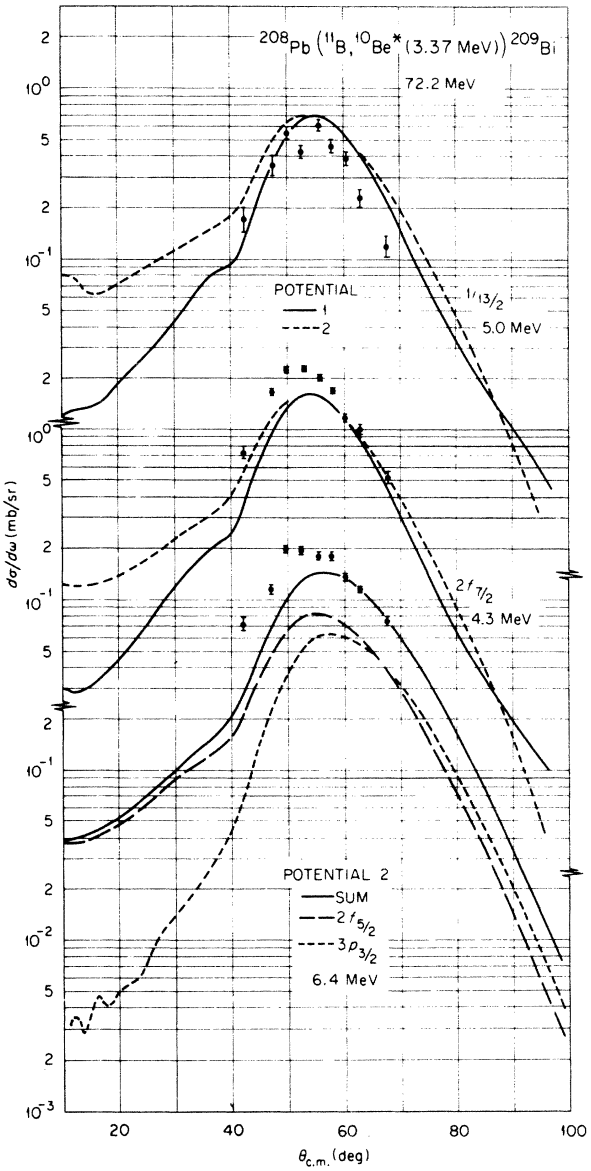

FIG. 10. Differential cross sections for groups from the (^{11}B, ^{10}Be*) reactions leaving ^{10}Be in its excited 2^+ state at 3.37 MeV. The curves are DWBA calculations normalized with the spectroscopic factors in Table VII and using potential 1 or 2 (see Table I) in both entrance and exit channels.

(about 12 fm in the present case); then L_a and L_b are those values for which the elastic scattering amplitude has $|\eta_{L_a}| \approx |\eta_{L_b}| \approx (2)^{-1/2}$. These may be found using the optical potentials which fit the elastic data.

The actual Q and L values for the transitions observed here are close to the optimum values except for the (^{11}B, ^{10}B) case where Q_{opt} is about −2 MeV instead of the actual $Q \simeq -7.5$ to −10 MeV and where $L_{opt} \approx 10$. The optimum Q corresponds to a state about 5 MeV below the ground state and the peaks in the spectrum (Fig. 4) show a general decrease with increasing excitation energy in agreement with this fact. The maximum L transfer allowed even for the $1j_{15/2}$ capture is 8, two units less than the optimum. Nonetheless, the peak intensities for the (^{11}B, ^{10}B) reactions (Figs. 4, 11) are still comparable to those for the other, better matched re-

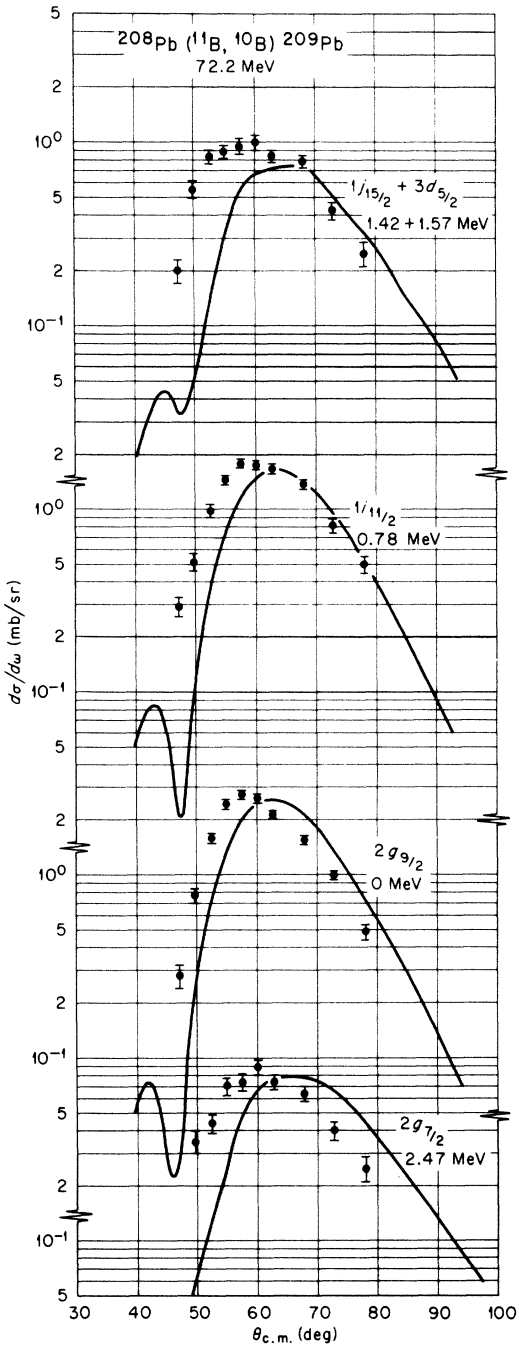

FIG. 11. Differential cross sections for groups from the (^{11}B, ^{10}B) reactions. The curves are DWBA calculations normalized with the spectroscopic factors in Table VIII and using potential 1 (see Table I) in both entrance and exit channels.

actions, although we shall see below that we encounter difficulties with the DWBA fits. This may indicate that higher order processes are contributing.

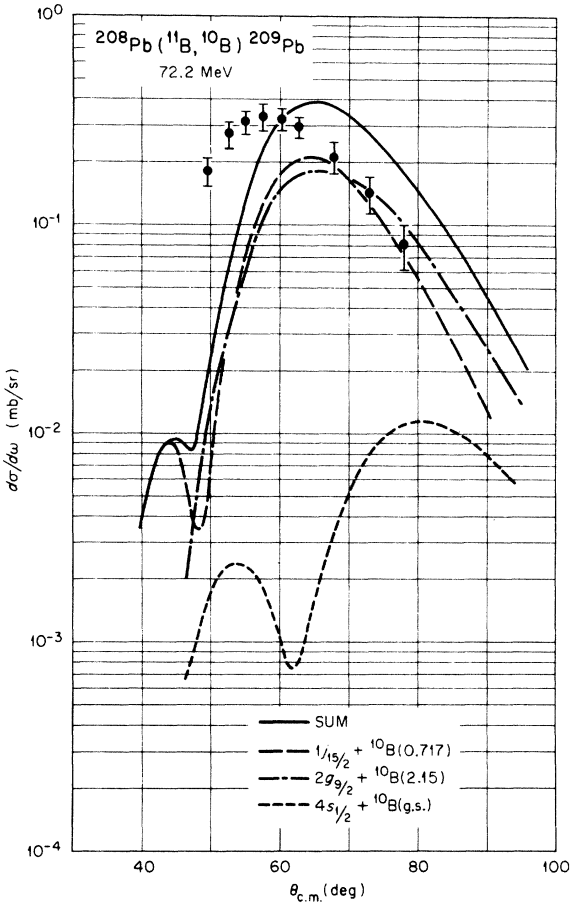

FIG. 12. Differential cross sections for the group near 2.1 MeV (see Fig. 4) from the (^{11}B, ^{10}B) reactions. The curves are DWBA calculations normalized with the spectroscopic factors in Table VIII for transfers leaving ^{10}B in its ground, 0.717-MeV, and 2.15-MeV excited states.

Brink[22] has proposed more detailed kinematical conditions to be met if the transfer probability is to be large. We have studied these also, but they do not seem to throw any further light on our present results. The quantity he calls Δk, arising from detailed momentum matching at the nuclear surface, is small for all the transitions, while his ΔL, due to angular momentum matching, gives essentially the same information as L_{opt} discussed above.

V. OPTICAL MODEL ANALYSIS OF ELASTIC DATA

The data for elastic scattering of 72.2-MeV ^{11}B (part of present investigation) and of 77.4- and 116.4-MeV ^{12}C (results of experiments reported in Ref. 1) from ^{208}Pb were fitted using the search code GENOA[23] in order to provide optical potentials for the DWBA analysis of the transfer reactions.

TABLE I. Optical potentials for $^{11}B+^{208}Pb$ at 72.2 MeV. Underlined values were kept fixed during the search.

Pot.	V (MeV)	W (MeV)	r_0 (fm)	a (fm)	σ_A (mb)
1	40	15	1.2177	0.612	1366
2	40	16.44	1.3029 [a]	0.424	1321
3	40	15	1.31	0.45	1468
4	40	4	1.2974	0.439	1335
5	200	75	1.0688	0.655	1371
6	21.78	2.01	1.3340	0.416	1281

[a] Radius of imaginary part fixed at $r_0' = r_0 - 0.15$ fm.

The usual Woods-Saxon form was chosen,

$$U(r) = -(V+iW)(e^x+1)^{-1},$$

where

$$x = (r-R)/a, \quad R = r_0(A_1^{1/3}+A_2^{1/3}),$$

together with the Coulomb potential from a uniform charge of radius $R_c = 1.3(A_1^{1/3}+A_2^{1/3})$ fm. The potential found at Berkeley[24] to fit $^{16}O+^{208}Pb$ was used as a starting point; these parameters are listed in Table I as potential 3. Figure 13 shows that this does not fit the ^{11}B data, although (Fig. 14) it already gives a good fit to the ^{12}C data. Varying only r_0 and a led to potential 1 and the fit shown in Fig. 13; this potential, however, does *not* give a good fit to the ^{12}C data (Fig. 14). There appears to be a significant difference between the data for the scattering of the two projectiles.

Allowing the well depths V and W to vary also produced no improvements in the fit to the ^{11}B data. Similar results were found for deeper potentials; e.g., potential 5 (Table I) gave scattering indistinguishable from potential 1. The main discrepancy with the ^{11}B data occurs at the rise above Rutherford scattering near 50°. Further improvements were sought by allowing the real and imaginary parts of the potential to have different radius and/or diffuseness parameters. A slightly better fit to the 50° region was obtained by making the imaginary radius smaller, as with potential 2 (Table I and Fig. 13).

The smallest deviation between experiment and optical model predictions was obtained by starting with the shallow potential used earlier[25] to describe the inelastic scattering of ^{11}B. This resulted in potential 6 (Table I), whose most obvious feature is the small imaginary part, $W/V \approx 0.1$. Besides producing the closest fit to the data (including near 50°), this potential also predicts oscillations in the elastic angular distribution, even for angles below 40°, with a period of a few degrees, which are similar to those recently suggested[26] as due to interference between the negative branch of the classical deflection function and the two positive branches. The present elastic data cannot rule out these oscillations; on the other hand, the inelastic and transfer cross sections predicted with this potential are completely at variance with the measured ones.

Good fits to the ^{11}B data were also obtained for potentials with W/V fixed at values ranging from 0.4 to 0.1, starting from potential 1. An example

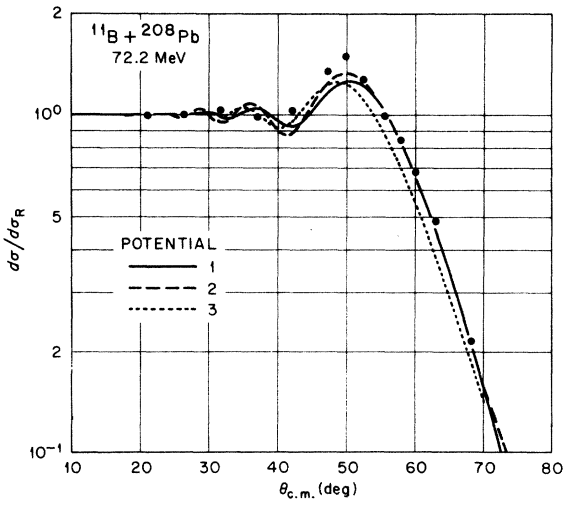

FIG. 13. Differential cross sections for elastic scattering of ^{11}B on ^{208}Pb with optical model curves corresponding to the potentials in Table I.

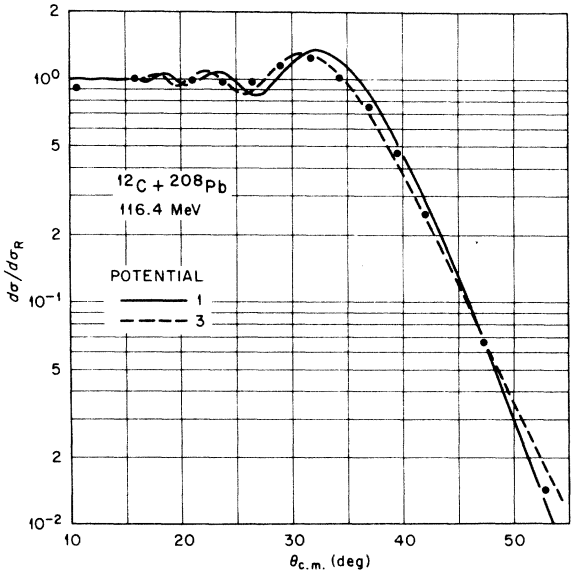

FIG. 14. Differential cross sections for elastic scattering of ^{12}C on ^{208}Pb with optical model curves corresponding to the potentials in Table I.

is potential 4 (Table I) and the fits are similar to those shown in Fig. 13. In each case, allowing V to vary also produced no improvement.

All the potentials found to fit the ^{11}B data have real parts which coincide near $r = 12.15$ fm with the value $-(1.02 \pm 0.05)$ MeV; this appears to be the most characteristic feature of the data. (Note that the Berkeley potential, potential 3 of Table I, has the value -1.45 MeV at this radius.) The imaginary parts do not share this feature, ranging in value at this strong absorption radius from -25 keV (potential 2) to -400 keV (potential 1). (It should be remarked, however, that these various potentials do not give *identical* scattering, but only equivalent fits to the available data. The corresponding partial wave scattering amplitudes η_L do differ. While all show the same general rise from $|\eta_L| \approx 0.1$ at $L \approx 30$ to $|\eta_L| \approx 0.9$ at $L \approx 40$, the η_L for the more weakly absorbing potentials like potential 4 do show more structure as a function of L.)

As Fig. 14 shows, potential 3 already gives a good fit to the ^{12}C data. Starting from this potential a best fit is obtained, keeping $V = 40$ MeV, with $W = 23.5$ MeV, $r_0 = 1.226$ fm, and $a = 0.607$ fm, parameters not very different from potential 1 except for the increase in W. Varying V led to no further improvement. These data were also subjected to analyses similar to those described above for ^{11}B, but the results will not be discussed here except to say that the higher energy 116.4-MeV data do show a marked preference for a deeper imaginary strength with $W/V \approx 0.5$ when $V \approx 40$ MeV. These data indicate that the real $^{12}C + ^{208}Pb$ potential is about -0.7 MeV at about 12.5 fm.

VI. DISTORTED-WAVE METHOD

The application of the distorted-wave Born approximation to transfer reactions induced by light ions has been discussed previously in some detail.[27,28] Here we will only stress those features of particular interest for heavy ions.

Consider the reaction $A(a, b)B$ [or its inverse, $B(b, a)A$] where $a = b + x$ and $B = A + x$ so that x is the transferred particle. (We use the notation of Satchler.[12,29]) The DWBA transition amplitude is then proportional to

$$\int d\vec{r}_{aA} \int d\vec{r}_{bB}\, \chi_{bB}^{(-)*}(\vec{k}_b, \vec{r}_{bB}) \langle \psi_B^*(\vec{r}_{xA})\psi_b | V | \psi_A \psi_a(\vec{r}_{xb}) \rangle \chi_{aA}^{(+)}(\vec{k}_a, \vec{r}_{aA}), \tag{3}$$

where (see Appendix) $\vec{r}_{ij}$ is the vector joining the centers of mass of particles i and j and we only show explicitly the coordinates of most interest.[12,29] Integration over the other coordinates is implied by the angular brackets. The χ_i are the usual distorted waves generated by optical potentials U_i, and ψ_i is the internal wave function for nucleus i. The interaction V in the post form is

$$V(\text{post}) = V_{bB} - U_{bB} = V_{bx} + V_{bA} - U_{bB}, \tag{4}$$

and in the prior form is

$$V(\text{prior}) = V_{aA} - U_{aA} = V_{xA} + V_{bA} - U_{aA}. \tag{5}$$

It is customary to take the leading terms only, namely the binding potentials,

$$V(\text{post}) \approx V_{bx}, \quad V(\text{prior}) \approx V_{xA}. \tag{6}$$

In the calculations reported here we use V(post) and take only the nuclear part of V_{bx}. We return to this point later.

The new features introduced by heavy ions (i.e., mass > 4) include:

(i) The particle x need not be in an S state relative to b when bound to form the state ψ_a of nucleus a. This complicates the angular momentum algebra.

(ii) It is not satisfactory to make the zero-range approximation, namely to use

$$V_{bx}\psi_a(\vec{r}_{xb}) \approx D_0 \delta(\vec{r}_{xb}). \tag{7}$$

Rather we must do the full finite-range calculation. (The impact of this requirement often has been reduced in the past by introducing the so-called no-recoil approximation.[12,29] This approximation is *not* made here.)

(iii) As a consequence of (ii), we need the form factor (or wave function) ψ_a of the b, x relative motion and the associated spectroscopic factor, as well as those for the $B = A + x$ system. This may introduce additional uncertainties. [In principle this is true of light-ion reactions also, but then the normalization constant required, D_0 in Eq. (7), can often be obtained with little error.]

(iv) The outgoing nucleus b [or a in the inverse $B(b, a)A$ reaction] may be in an excited state.

(v) The calculation may be changed in trivial but important ways, namely much larger numbers of partial waves may have to be included, and numerical accuracy may demand much smaller (and hence many more) steps in the radial integrations. It then becomes important to devise techniques to reduce the additional computational time that is implied.[13,14] (See Appendix.)

A. Selection rules

If the transferred particle is in an orbit in nucleus a with orbital angular momentum l_a and total angular momentum j_a, and in an orbit in nucleus B with l_B and j_B, then the angular momentum

transfer L is limited by

$$|j_a - j_B| \leq L \leq j_a + j_B \tag{8a}$$

and

$$|l_a - l_B| \leq L \leq l_a + l_B . \tag{8b}$$

The cross sections for different L transfers add incoherently. In the present case, their angular distributions are almost identical.

In general L need not be tied to the parity change $\Delta\pi$. Terms with L for which $\Delta\pi = (-)^L$ are referred to as having "normal" parity, those for which $\Delta\pi = (-)^{L+1}$ as nonnormal parity. (The latter vanish if the zero-range or no-recoil approximations are made.)

In our case, x is a nucleon and $j_i = l_i \pm \frac{1}{2}$. Then l_B and j_B refer to the orbit in which x is added to (or picked up from) ^{208}Pb. Since ^{208}Pb has zero spin in its ground state, there is a unique j_B for each transition. The quantum numbers l_a and j_a refer to the orbit in which x is picked up from (or added to) ^{11}B. If the resulting nucleus has spin 0, then j_a also has a unique value. Otherwise, more than one value is allowed (although, in the absence of spin-orbit coupling in the distorted waves, the cross sections for different j_a add incoherently). For example, in the (^{11}B, ^{12}B) reaction, the ^{12}B ground state has spin 1^+ and $p_{1/2}$, $p_{3/2}$, and $f_{5/2}$ capture is allowed. Structure considerations suggest that occupation of the $1f_{5/2}$ orbit in the ^{12}B ground state is negligible so that we need only consider $l_a = 1$, $j_a = \frac{1}{2}$ or $\frac{3}{2}$. Similarly, in (^{11}B, ^{10}B) transfers, although the ^{10}B ground state is 3^+ and $l_a = 3$ is allowed, we are justified in neglecting it and considering only $l_a = 1$, $j_a = \frac{3}{2}$. Reactions leading to excited states of the light nucleus with nonzero spin may also allow more than one j_a value.

Since for the reactions considered here we have $l_a = 1$, rule (8b) allows $L = l_B$, $l_B \pm 1$. When allowed, the largest $L = l_B + 1$ predominates and typically the $L = l_B - 1$ and the nonnormal $L = l_B$ have cross sections which are an order of magnitude smaller. However, if $L = l_B + 1$ is forbidden by rule (8a), the nonnormal $L = l_B$ can contribute a large fraction of the cross section. This occurs if $(l_a, j_a) = p_{1/2}$ and $j_B = l_b - \frac{1}{2}$. A neutron captured on ^{11}B to form the ground state of ^{12}B enters the $1p_{1/2}$ orbit with about 85% probability. With this component, the nonnormal L contributes about 30% of the cross section for pickup of $3p_{1/2}$ from ^{208}Pb and about 40% of the cross section for pickup of $2f_{5/2}$. (These contributions would be absent from a no-recoil calculation.) However, the remaining 15% of $1p_{3/2}$ capture into ^{12}B contributes disproportionately to these transitions because transfer between $j_a = l_a + \frac{1}{2}$ and $j_B = l_B - \frac{1}{2}$ (or between $j_a = l_a - \frac{1}{2}$ and $j_B = l_B + \frac{1}{2}$) is strongly favored over the other alternatives which require a spin-flip.[30] The net result is that the nonnormal L contributes about 21% of the total $3p_{1/2}$ cross section and about 17% of the total $2f_{5/2}$ cross section.

B. Bound-state wave functions

We assume that the wave function of the nucleon x before and after transfer is the appropriate eigenfunction for a Woods-Saxon well, plus a spin-orbit coupling term, with a binding energy equal to the corresponding experimental separation energy.

This is a reasonable approximation for the "single-particle" or "single-hole" states excited in ^{208}Pb because of its closed shell nature. Nonetheless, there remain uncertainties in the values to be used for the parameters of this well. For the ^{208}Pb ± proton system we have chosen to use the parameters (Table II) which reproduce the single particle and hole energies and also give a charge distribution in good agreement with electron scattering measurements.[31] These parameters also give reasonable results for (^{3}He, d) and (d, ^{3}He) measurements[28] (see below). We used neutron parameters (Table II) derived from sub-Coulomb stripping measurements[32]; these also give good agreement with (d, t) measurements[28,33] on ^{208}Pb.

The correct choice of these parameters is important in determining the absolute magnitudes of the cross section, although the angular distributions are insensitive to them. For example, using the neutron potential (Table II) for the *protons* almost halves the predicted cross sections (and consequently greatly increases the extracted spectroscopic factors). Varying the spin-orbit term in the binding potential produces j-dependent effects, especially changing the relative cross sections for spin-orbit partners with $j = l \pm \frac{1}{2}$. Of

TABLE II. Parameters for bound-state potential wells.

System	V [a] (MeV)	r_0 [b] (fm)	a (fm)	V_{so} (MeV)	r_{so} [b] (fm)	a_{so} (fm)	r_c [c] (fm)
^{208}Pb + p	≈60	1.28	0.76	6.0	1.09	0.60	1.20
^{208}Pb + n	≈45	1.25	0.63	7.0	1.10	0.50	
^{11}B ±1	V [a]	1.35	0.50	$\lambda = 20$ [d]	1.35	0.50	1.35

[a] Adjusted to give a binding B equal to the experimental separation energies; B = 11.456 MeV for ^{10}B + n, B = 11.228 MeV for ^{10}Be + p, B = 3.369 MeV for ^{11}B + n, B = 15.957 MeV for ^{11}B + p.

[b] Radii defined as $R = r_0 A^{1/3}$ where A is the mass number of the core to which the nucleon is bound.

[c] Coulomb potential from a uniform charge distribution of radius $r_c A^{1/3}$.

[d] Spin-orbit coupling of λ times the Thomas term.

course, it is also an approximation to assume that the same potential well is suitable for all the orbits. Hartree-Fock studies[34] show that the equivalent local potential may vary significantly from orbit to orbit; for example, it has been suggested that the diffuseness should be larger for the low l neutron orbits than for those with high l. Our value of $a = 0.63$ fm is appropriate for the latter. If, as suggested,[34] we change a to 0.84 fm for the $3p$ neutrons in ^{208}Pb, the (^{11}B, ^{12}B) pickup cross section is increased by a factor of 1.56 for both $3p_{1/2}$ and $3p_{3/2}$.

This sensitivity is very similar to that found for light-ion reactions[28,32,33] and occurs because the reaction (because of the Coulomb barrier or because of strong absorption) is peripheral and is only sensitive to the tail of the bound state wave function. The *shape* of the tail is determined by the binding energy, consequently the reaction cross section is simply proportional to the square of the normalization of the tail. (This is especially evident in the theory of sub-Coulomb transfers.[30,33]) Hence, instead of separating the nuclear overlap into the product of a spectroscopic amplitude times a single-particle wave function (which is a theoretical artifact), we may extract directly from experiment the normalization of the form factor tail. This number, which is related to the reduced width for the transition, will then be independent of the binding well parameters used, provided the post form (6) of the interaction is used. This has been done previously[28,33] for pickup from ^{208}Pb, and we also use this approach below.

We also have to adopt a binding potential V_{bx} to give the wave function for the nucleon in the light system, $^{11}\mathrm{B} \pm 1$. The cross section magnitudes are sensitive to this choice also, although the *relative* cross sections for different $^{208}\mathrm{Pb} \pm 1$ states tend to be unaffected provided the same $^{11}\mathrm{B} \pm 1$ wave function is involved in each of them. If we use the post-interaction form (6) we cannot avoid explicitly defining V_{bx} and the reaction amplitude does not simply depend only on the asymptotic part of the wave function. The appearance of the product $V_{bx}\psi_a(\vec{r}_{xb})$ in the amplitude (3) ensures that important contributions come from within the surface region of the $^{11}\mathrm{B} \pm 1$ system. [In the (^{11}B, ^{10}Be) reaction feeding the $3p_{3/2}$ state in ^{209}Bi, the integrand for transfer along the line of centers, when they are separated by the strong absorption radius of about 12 fm, peaks at $r_{xb} \approx 2.2$ fm with a width of about 2 fm, while the radius of the potential well V_{bx} is 2.91 fm.]

The potential chosen for the light system (Table II) was based upon a study[35] of the sizes of $1p$-shell nuclei. It generates a charge distribution for ^{12}C which has (after correction for center of mass recoil) a root mean square radius of 2.51 fm. This is to be compared to the latest experimental value[36] of 2.462 ± 0.022 fm. Consequently a somewhat smaller well might be better; the popular choice of $r_0 = 1.25$ fm, $a = 0.65$ fm gives an rms radius of 2.46 fm for ^{12}C. Fortunately, Table III indicates that this would only change the transfer cross sections by about 6%. A third choice, $r_0 = 1.15$ fm, $a = 0.55$ fm, based upon an optical potential for proton scattering from $1p$-shell nuclei[37,38] gives a smaller rms radius of 2.33 fm for ^{12}C and appreciably smaller transfer cross sections (Table III). [Similar results were found for the (^{11}B, ^{12}B) reaction.]

It is assumed the neutron wave functions for the light system can be generated in the same well as the protons. It is also assumed that the well radius is proportional to $A^{1/3}$, where A is the mass number of the core to which the nucleon is bound. There is some evidence[35] that the well is almost independent of A for $1p$-shell nuclei, and this introduces a further small uncertainty.

C. Spectroscopic factors

The cross section is proportional to the product of the spectroscopic factors $\mathcal{S}_a\mathcal{S}_B$ for the $a = b + x$ and $B = A + x$ partitions, respectively. (We use here the abbreviated notation $\mathcal{S} = C^2S$, where C is the usual isospin Clebsch-Gordan coefficient.) For stripping on to ^{208}Pb we expect $\mathcal{S}_B = 1$ for pure single-particle states, while pickup from a j orbit gives $\mathcal{S}_B = 2j + 1$ for pure single-hole states. In practice some of these states will mix with nearby core-excited states, depleting their strength. Some of the weak fragments from this mixing have been identified in light-ion measurements, and theoretical calculations[39,40] can account for the mixing qualitatively.

Values of $\mathcal{S}_B$ for the states observed here have

TABLE III. Variation of ^{208}Pb(^{11}B, ^{10}Be)^{209}Bi ($3p_{3/2}$) cross section with variation of $^{11}\mathrm{B} + ^{10}\mathrm{Be} + p$ binding potential parameters.

V [a] (MeV)	r_0 (fm)	a (fm)	V_{so} (MeV)	σ_{peak} [b]	$\mathcal{S}_a\mathcal{S}_B$ [b]	$\langle r^2 \rangle^{1/2}$ [c] (fm)
50.84	1.35	0.50	5.6	1.0	1.0	2.51
50.27	1.35	0.50	5.9 [d]	0.95	1.05	2.49
63.95	1.15	0.55	5.3	0.72	1.395	2.33
58.08	1.25	0.65	5.5	1.065	0.94	2.46

[a] Depth to bind $1p_{3/2}$ proton by 11.228 MeV.

[b] Normalized to unity for first case.

[c] Predicted root mean square radius for charge distribution of ^{12}C.

[d] Smaller radius for spin-orbit term, $r_{so} = 1.15$ fm.

been obtained by analyses of light-ion measurements.[28,32,41-47] These, of course, are subject to the same kinds of uncertainties as are being discussed here. It is important, for example, that these analyses should be made using the same bound state wave functions; for this reason some of the measurements were reanalyzed. Uncertainties in the $\mathcal{S}_B$ due to reasonable optical potential, normalization (values of D_0), finite-range and nonlocality uncertainties are of the order of 20%.

The factors $\mathcal{S}_a$ for the $^{11}\mathrm{B}\pm1$ system are somewhat uncertain. The $1p$-shell model analysis of Cohen and Kurath[48] (CK) provides a guide (see Table IV). We may also appeal to light ion stripping and pickup experiments involving ^{11}B. Unfortunately, the understanding of these reactions on very light nuclei is beset with uncertainties and a considerable range of empirical $\mathcal{S}_a$ values may be available. Often they are deduced using bound state wells different from that used here; sometimes the bound state well is not even specified. Rather than attempt a consistent reanalysis of these data, we simply give in Table IV the range of $\mathcal{S}_a$ values quoted.[37,49-56]

The $\mathcal{S}_a$ quoted for neutron pickup from ^{11}B is almost twice the theoretical value, but only one experiment is available and the neutron bound state parameters are not quoted. The analyses of proton pickup use bound state parameters similar to those used here and the results for $\mathcal{S}_a$ are consistently larger than the theoretical value. Stripping a neutron on to ^{11}B gives a result consistent with the theory. Stripping a proton gives a wide range of values; however, a careful examination of the analyses suggests that the experimental $\mathcal{S}_a$ is either equal to or somewhat less than the theoretical value of 2.85; say between 2.5 and 3.0.

D. Interaction and post-prior discrepancy

The nuclear part of the first term, V_{bx}, of the post-interaction form (4) was used for the calculations presented here. The V_{bx} is the potential well used to generate the bound state wave function for the $^{11}\mathrm{B}\pm1$ system. The expectation value of the spin-orbit term of this potential was included; some authors (for example, Refs. 13 and 14) neglect this term. In the (^{11}B, ^{10}Be) reaction, including this term (attractive for the $1p_{3/2}$ proton) increased the cross section by 15%. The other reactions will be increased also, except for (^{11}B, ^{12}B) where the predominantly $1p_{1/2}$ capture should lead to a small decrease.

If all the terms of Eqs. (4) and (5) were included, the post and prior forms would give the same result. This equivalence no longer holds when only the leading terms are taken. For example, for the $3p_{3/2}$ and $2f_{7/2}$ transfers in the (^{11}B, ^{10}Be) reaction we find that the nuclear part of V_{xA} in the prior form gives cross sections 1.6 times larger than the nuclear part of V_{bx} in the post form. Neutron transfer is less affected; $3p_{3/2}$ pickup in the (^{11}B, ^{12}B) reaction using the prior form is 20% smaller than using the post form. This already suggests that the post-prior discrepancy is due more to neglect of the Coulomb terms than to neglect of the nuclear parts of the optical potentials U_{bB} or U_{aA}. Indeed, repeating the calculations with *all* the Coulomb interactions switched off leads to agreement between post and prior to within 1% at the peak.

Including just the Coulomb part of V_{bx} for proton transfers reduces the cross sections by about 20%, but including the Coulomb part of V_{xA} has a dramatic effect, reducing the cross section by more than an order of magnitude. Examination of the form of the remaining terms shows that they will largely cancel this latter effect and somewhat reduce the former. This expectation has now been confirmed and is reported on elsewhere.[57]

Including the optical potential terms again reduces the cross sections[57] by about 10%. The remaining term of the interaction, namely V_{bA}, appears in both post and prior forms and is not very well specified. Calculations have been made[58] assuming that it can be replaced by the optical potential appropriate for the $b+A$ system. Almost no change in angular distribution was found, but some change in magnitude. Calculations have not been made for reactions like those of interest here. However, since these reactions are confined to the vicinity of the strong absorption radii, the argument of V_{bA} has values $r_{bA}\approx 12$ fm and V_{bA} has a much smaller value (~ -1 MeV) than the values of V_{bx} (~ -30 MeV) which contribute strongly. Further, there is considerable cancellation between V_{bA} and the optical potential terms U_{bB} or U_{aA} in Eqs. (4) and (5), and since the latter only have about 10% effect here,[57] the net result should be small.

These problems are being investigated further.

TABLE IV. Spectroscopic factors $\mathcal{S}_a$ for $^{11}\mathrm{B}\pm1$ system.

System	Orbit	CK[a]	Expt.	Refs.
$^{11}\mathrm{B}=^{10}\mathrm{B}+n$	$1p_{3/2}$	1.09	1.9	49
$^{11}\mathrm{B}=^{10}\mathrm{Be}+p$	$1p_{3/2}$	0.43	0.65–0.90	49, 50, 51
$^{12}\mathrm{B}=^{11}\mathrm{B}+n$	$1p_{3/2}$ $1p_{1/2}$	0.12 0.71	0.7[b]	52
$^{12}\mathrm{C}=^{11}\mathrm{B}+p$	$1p_{3/2}$	2.85	1.6–3.3	37, 53, 54, 55, 56

[a] Cohen and Kurath, Ref. 48.

[b] Assumed to be $1p_{1/2}$ only.

Suffice it to say here that we believe that using only the nuclear part of V_{bx} gives results accurate to about 20% for proton transfers and is much more accurate for neutron transfers.

E. Optical potential ambiguities

Optical potentials for the entrance channel were determined by fitting elastic data (Sec. V above). Unfortunately, there are no data for the exit channels; the closest we have is for $^{12}C+^{208}Pb$. We do not feel justified in arbitrarily varying parameters for the exit channel, so we choose to assume the same potential as in the entrance channel, except for the (^{11}B, ^{12}C) reaction where calculations were also made using in the exit channel the potential 3 of Table I which does fit $^{12}C + ^{208}Pb$ scattering (Fig. 14).

Even so, we saw above that the elastic data do not determine the ^{11}B potential unambiguously and this leads to uncertainties in the transfer analysis. Figure 15 shows some calculations for the (^{11}B, ^{10}Be) reaction with various optical potentials from Table I used in both channels. Potential 6 can be ruled out immediately as incompatible with the data (Fig. 9). Potential 6 also gives inelastic scattering cross sections which oscillate rapidly with angle and which are at variance with the measurements.[25] Potential 4 agrees with the transfer data except at 37° and yields spectroscopic factors about 30% larger than does the use of potentials 1 and 5. Potential 4 also predicts rapid oscillations in the inelastic angular distributions but they are of small amplitude and are not conclusively in disagreement with the measurements. (Results similar to Fig. 15 are predicted for the other reactions when the "weakly" absorbing potentials are used.) It was decided, somewhat arbitrarily, not to use potential 4 for the main analyses.

Potentials 1 and 5, although having very different parameter values, give almost identical transfer cross sections. Calculations for the remaining potential of Table I, potential 2, are compared with those for potential 1 in Figs. 8 and 9. Potential 2 gives cross sections which peak a degree or two more forward than potential 1, and yields somewhat larger spectroscopic factors [by 30% or so for (^{11}B, ^{10}Be) and by about 10% for (^{11}B, ^{12}B)]. The angular distributions from potential 2 are in better agreement with the data.

Use of potential 3 for the ^{12}C channel in the (^{11}B, ^{12}C) reactions (Fig. 7) also gives smaller cross sections which peak at a slightly smaller angle than obtained with potential 1 in both channels. The spectroscopic factors are thus increased by about 60%, and the angular distributions again are in better agreement with the data. Other optical potentials which *optimize* the fit to the $^{12}C+^{208}Pb$ elastic data at 116.4 MeV give transfer results which are intermediate between those shown for potentials 1 and 3.

In light-ion reactions it is common to apply correction factors to the distorted waves generated by local optical potentials in the belief that the "true" potentials are nonlocal.[28] In general this remains true for heavy ions also, but the nonlocality is probably sufficiently small[59] that its effects can be neglected.

F. Multistep processes

Use of the DWBA implies a belief that only a one-step direct process is important. In general, multistep processes may contribute, for example, inelastic scattering before and after the transfer.[10] One suspects that excitation of ^{208}Pb has minimal effects for the strong single-particle (or -hole) states being studied here, but excitation of the light ion may be more likely. When the direct process is inhibited, for example, in the way that the (^{11}B, ^{10}B) reaction to the low-spin states in

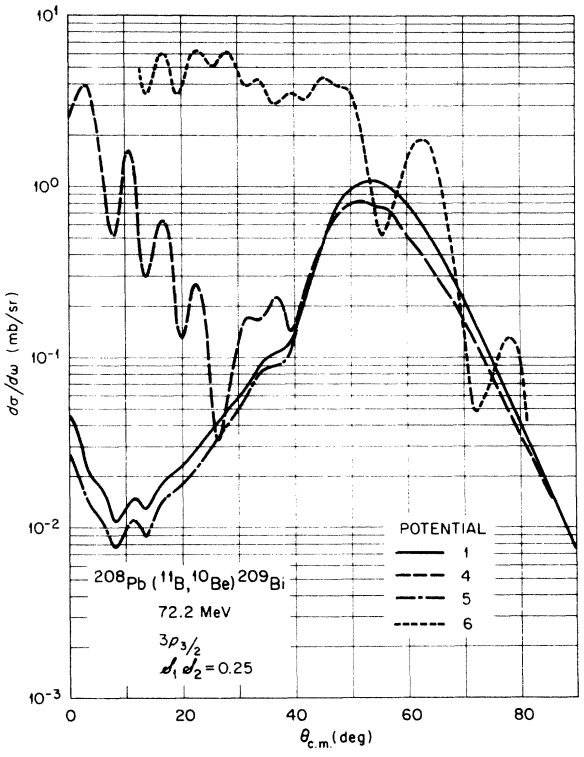

FIG. 15. DWBA calculations for the (^{11}B, ^{10}Be) reaction populating the $3p_{3/2}$ state at 3.12 MeV in ^{209}Bi. Various optical potentials from Table I were used in these calculations; however, in each instance the same potential was utilized in both entrance and exit channels.

^{209}Pb is inhibited by momentum mismatching, the opportunity for multistep processes to be important is enhanced. Currently we do not have the facility for calculating these effects. However, the spectra observed [especially for the (^{11}B, ^{10}Be) reaction where the spectrum spanned 20 MeV in excitation], show predominantly the single-particle or -hole states without other strong groups except for some excited states of the lighter ion. This suggests that excitation of the heavy system, at least, is not very important. If the angular distributions of the multi- and one-step processes differ sufficiently (as they do, apparently, in some cases[10]) it might be possible to get an indication of their importance from deviations between the angular distributions measured and those predicted by the one-step process. Possibly one place to look would be at the angle of the deep minimum near 45° in the (^{11}B, ^{12}B) reactions (see Fig. 8).

VII. DWBA ANALYSIS OF TRANSFER DATA

The DWBA calculations were made using the code LOLA[12] adapted for the IBM-360 computers at Oak Ridge. In most cases it was found to be adequate to include only partial waves with $\leq 80\hbar$ and to integrate out to 20 fm; further, contributions from radii r_{aA} and r_{bB} less than 8 fm, and partial waves with less than $20\hbar$ usually could be neglected. (It should be stressed that this is done to save computing time because these contributions are negligible–see Appendix. It is *not* analogous to the radial cutoff sometimes used in calculations of light-ion reactions.[28]) Exceptions occurred for the (^{11}B, ^{10}B) reaction, where there is a bad mismatch between entrance and exit channels and also when the more weakly absorbing potentials, potentials 4 and 6, were used. In these cases no cutoffs were used and up to 120 partial waves were included. Further details of the calculation are given in the Appendix.

A. ^{208}Pb(^{11}B,^{12}C)^{207}Tl reaction

There is a good matching between entrance and exit channels in this reaction so the conditions are favorable for the DWBA; $Q_{opt} = 6.8$ MeV and $L_{opt} \approx 1$ to 3. Figure 7 includes curves calculated in the DWBA. The solid curves use optical model potential 1 in both channels, while the dashed curves substitute potential 3 for the ^{12}C exit channel. This latter results in a slight shift forward of the peak, the shift increasing slightly with increasing excitation energy, i.e., decreasing Q value, and brings the calculations into somewhat better agreement with the data. A similar effect was seen by Low and Tamura[14] for the ^{208}Pb-(^{12}C, ^{11}B) reaction, but in their case it was obtained by making the ^{11}B potential have a *larger* radius than the ^{12}C potential, the opposite to what we have here.

The spectroscopic factor products $\mathcal{S}_a\mathcal{S}_B$ corresponding to the curves in Fig. 7 are listed in Table V. The changes in $\mathcal{S}_a\mathcal{S}_B$ due to other choices of normalizing to the data are obtained simply by scaling since the predicted cross section is proportional to $\mathcal{S}_a\mathcal{S}_B$. Also given are the values of $\mathcal{S}_B$ if we assume the CK value[48] of $\mathcal{S}_a = 2.85$.

$\mathcal{S}_B$ has also been obtained from (d, ^{3}He) measurements. In the analysis of the 50-MeV data[28] a bound-state potential was used equal to the *neutron* potential of Table II and it was concluded that the proton potential should have a larger radius. This was confirmed by the analysis of the 80-MeV results.[41] The 50-MeV data have been reanalyzed using the same proton potential as adopted here (Table II). The values of $\mathcal{S}_B$ given in Table V were obtained by including the effects of nonlocality of the distorting potentials and of finite range, cal-

TABLE V. Spectroscopic factors for ^{208}Pb(^{11}B, ^{12}C)^{207}Tl reactions.

Orbit	E_x (MeV)	Allowed L	Present experiment ^{12}C: Pot. 1 $\mathcal{S}_a\mathcal{S}_B$	$\mathcal{S}_B$ [a]	^{12}C: Pot. 3 $\mathcal{S}_a\mathcal{S}_B$	$\mathcal{S}_B$ [a]	Other $\mathcal{S}_B(d,{}^3\mathrm{He})$ [b]	Theory $\mathcal{S}_B$ [c]	$(2j+1)$	$u_{l_Bj_B}{}^2(r=10\text{ fm})$ [d] (10^{-4} protons fm^{-3})
$3s_{1/2}$	0.0	1	3.7	1.3	6.1	2.1	2.1	1.9	2	0.3764
$2d_{3/2}$	0.35	1,2,3	5.4	1.9	9.1	3.2	3.8	3.8	4	0.2539
$2d_{5/2}$	1.674	1,2,3	8.1	2.8	12.5	4.4	5.1	4.5	6	0.2140
$1h_{11/2}$	1.34	4,5,6	20.0	7.0	32.0	11.2	11.3	10.1	12	0.0905
$R_2 = d_{5/2}/d_{3/2}$			1.50		1.37		1.35	1.18	1.50	

[a] Assuming $\mathcal{S}_a = 2.85$ (Ref. 48).

[b] Reanalysis of data of Ref. 28, including nonlocality corrections to distorted waves and finite range, using the same proton wave functions as in present analysis.

[c] From Ref. 40.

[d] Proton wave function using potential from Table II.

TABLE VI. Spectroscopic factors for ^{208}Pb(^{11}B, ^{12}B)^{207}Pb reactions.

Orbit	E_x (MeV)	Allowed L [a]	Present experiment $\mathcal{S}_B$(Pot. 1) [b]	$\mathcal{S}_B$(Pot. 2) [b]	Other experiments $\mathcal{S}_B(d,t)$ [c]	$\mathcal{S}_B(p,d)$ [d]	$\mathcal{S}_B(d,t)$ [e]	$\mathcal{S}_B(^{12}C, ^{13}C)$ [f]	Theory $\mathcal{S}_B$ [g]	$(2j+1)$	$u_{l_B j_B}^2$ (r=10 fm) [h] (10^{-4} neutrons fm^{-3})
$3p_{1/2}$	0.0	0^1, 1, (2)	2.4	2.6	1.5	2.0±0.2	2.07	1.7 ±0.1	1.9	2	2.120
$3p_{3/2}$	0.90	(0), 1, 2	6.5	6.9	3.1	3.6±0.3	3.94	2.8 ±0.4	3.7	4	1.750
$2f_{5/2}$	0.57	2, 3, (4)	6.6	7.4	3.9	5.8±0.5	5.07	5.3 ±0.3	5.6	6	1.071
$2f_{7/2}$	2.34	(2), 3, 4	6.7	7.7	5.3	5.2±0.7	5.93	3.0 ±0.3	5.6	8	0.760
$R_1 = p_{3/2}/p_{1/2}$			2.7	2.7	2.05	1.8±0.2	1.90	1.6 ±0.2	1.9	2.00	
$R_3 = f_{7/2}/f_{5/2}$			1.02	1.04	1.35	0.9±0.2	1.17	0.58±0.06	1.0	1.33	

[a] Values in parentheses only allowed with $1p_{3/2}$ capture into ^{12}B.
[b] Assuming (Ref. 48) $\mathcal{S}_a(1p_{1/2}) = 0.71$, $\mathcal{S}_a(1p_{3/2}) = 0.12$ for $^{12}B = {}^{11}B + n$.
[c] Reanalysis of data of Ref. 28 including nonlocality effects on the distorted waves and finite range, using same neutron wave function as in present analysis.
[d] Average of results from Refs. 42–44, using similar neutron wave functions except that $r_{so} = r_0$, $a_{so} = a$.
[e] From Ref. 33, using our neutron wave functions.
[f] From Ref. 14, using a neutron binding well similar to our *proton* potential (Table II); this *underestimates* $\mathcal{S}_B$ by roughly a factor of 2. $\mathcal{S}_a = 0.63$ assumed (Ref. 48) for $^{13}C = {}^{12}C + n$. Average for three energies.
[g] From Ref. 40.
[h] Neutron wave function using potential from Table II.
[i] Not allowed for $1p_{3/2}$ capture into ^{12}B.

culated in the local energy approximation.[28] [Nonlocality, with $\beta_d = 0.54$ fm and $\beta_3 = 0.3$ fm, has a 1% effect, while finite-range (range 1.6 fm) reduces the $\mathcal{S}_B$ uniformly by 17%.]

Using potential 3 in the ^{12}C channel makes the present $\mathcal{S}_B$ closer to $(2j+1)$ and also in remarkably good agreement with the $(d, {}^3\mathrm{He})$ values. In view of all the uncertainties discussed earlier, this agreement has to be somewhat fortuitous. The deviations from $(2j+1)$ can be understood qualitatively in terms of the mixing of the hole states with adjacent core-excited states of the same spin and parity. Some theoretical estimates of Ring and Werner[40] are included in Table V and similar results have been obtained by Hamamoto.[39] Experimentally the ratio R_2 of $d_{5/2}$ to $d_{3/2}$ is closer to the unperturbed value than is predicted.

The ^{12}C spectrum (Fig. 5) also shows groups which would correspond to transfers in which the ^{12}C was emitted in its 4.43-MeV 2^+ excited state. It is estimated that the two groups marked have peak cross sections of about 0.5 mb/sr. The corresponding groups associated with the ^{12}C ground state have peak cross sections (Fig. 7) of about 1.1 and 0.7 mb/sr; i.e., the excited state groups are almost as intense as the ground state groups. The light-ion spectroscopic factor $\mathcal{S}_a$ favors the ground state of ^{12}C. The Cohen-Kurath theoretical predictions give $\mathcal{S}_a(^{12}C_{gs})/\mathcal{S}_a(^{12}C^*) \approx 5.2$. Experimental light-ion stripping[53, 55, 56] on ^{11}B gives values for this ratio ranging from 2.2 to 7. However, this factor is compensated for by the statistical weight factor of $2s_a + 1 = 5$ from the spin of the ^{12}C* compared to $2s_a + 1 = 1$ for the ground state. The Q values are less favorable for ^{12}C* and this would lead to some reduction in cross section. Consequently the observed cross sections for ^{12}C* appear to be compatible with those expected for a one-step transition. More detailed experimental and theoretical results would be required to determine whether inelastic excitation of the ^{12}C plays a role.

B. ^{208}Pb(^{11}B,^{12}B)^{207}Pb reaction

Again there is good matching between entrance and exit channels; $Q_{opt} = -2.2$ and $L_{opt} \approx 1$ to 3. In this case, the neutron in ^{12}B may be in the $1p_{1/2}$ or $1p_{3/2}$ orbits. In the absence of direct information we assumed the CK values[48] of $\mathcal{S}_a(1p_{1/2}) = 0.71$, $\mathcal{S}_a(1p_{3/2}) = 0.12$. The ratio of these is very important in determining the ratios of $j_B = l_B + \frac{1}{2}$ to $j_B = l_B - \frac{1}{2}$ pickup from ^{208}Pb because of the inhibition of transfers which require a spin-flip.[30]

Figure 8 shows DWBA curves obtained by using either optical potential 1 or potential 2 in both channels and Table VI lists the corresponding $\mathcal{S}_B$

values. The data are fitted quite well, with a preference for potential 2 which gives peaks about 2° more forward than potential 1 and which fits better the data points at 37°. The spectroscopic factors obtained with the two potentials differ by only about 10%. A striking feature of the predicted angular distributions is the deep minimum which occurs near 45°. The data points at 37 and 42° are in agreement with a minimum here. [The other neutron transfer, (^{11}B, ^{10}B), also shows a minimum in this region, although it is not as well developed as here. In the proton transfers, this feature appears simply as a shoulder on the side of the main peak.]

Other measures of $\mathcal{S}_B$ obtained from (d, t) and (p, d) experiments[28,33,42-44] are included in Table VI; these were obtained using the same or similar neutron wave functions as are used here. While the two light-ion measurements agree fairly well, the heavy-ion results give consistently larger spectroscopic factors. This might be due to an incorrect choice of ^{12}B optical potential. The $\mathcal{S}(j_B = l_B + \frac{1}{2})/\mathcal{S}(j_B = l_B - \frac{1}{2}) = R_{l_B}$ ratios vary appreciably in the different reactions. The light-ion measurements agree for R_1 but not R_3. Our present results for ^{11}B give too large a value for R_1, while R_3 is acceptable. This discrepancy cannot be resolved by changing the relative amounts of $1p_{1/2}$ and $1p_{3/2}$ capture into ^{12}B. The CK mixture[48] gives (Table VI) $R_1 = 2.7$, $R_3 = 1.0$. If we had chosen pure $1p_{1/2}$ capture we would have got $R_1 = 2.1$, $R_3 = 0.53$, while pure $1p_{3/2}$ yields $R_1 = 6.75$, $R_3 = 8.3$. Hence any change which improves the light- and heavy-ion agreement for R_1 worsens it for R_3, and vice versa.

Theoretical estimates[39,40] of $\mathcal{S}_B$ are also included in Table VI; the predicted R_1 agrees with the light-ion work, the predicted R_3 agrees with the heavy-ion data.

There is a fairly close coincidence in energy between the $3p_{3/2}$ group and the $3p_{1/2}$ pickup with ^{12}B excited to its 0.953 MeV, 2^+ state. (This alternative is not to be confused with a two-step process in which the ^{12}B is excited *after* the transfer has taken place. It is a direct one-step process in which the capture takes place into the excited state of ^{12}B.) An estimate of this possible contaminant was made using the CK values[48] for the $\mathcal{S}_a$ for this excited ^{12}B state. With these assumptions, it would be possible for 17% of the "$3p_{3/2}$" group to come from this contaminant. If this amount of contaminant were present, R_1 would be reduced to 2.25, in better agreement with the light-ion results.

The states seen here were also excited in the (^{12}C, ^{13}C) reaction[1] and the results analyzed in a similar way by Low and Tamura.[14] Their values of $\mathcal{S}_B$ are also listed in Table VI. Unfortunately they use a binding potential for the neutrons in ^{208}Pb similar to our *proton* potential (except that $r_{so} = r_0$, $a_{so} = a$) and the larger radius of this potential means their $\mathcal{S}_B$ should be multiplied by roughly a factor of 2 before being compared to ours. Adopting our spin-orbit geometry would also increase their R_1 and R_3 ratios somewhat.[28] These changes would then bring their numbers for $\mathcal{S}_B$ into quite good agreement with ours.

C. ^{208}Pb(^{11}B, ^{10}Be)^{209}Bi reaction

Here also the matching of entrance and exit channels is quite good ($Q_{opt} = -11.4$, $L_{opt} \approx 1$ to

TABLE VII. Spectroscopic factors for ^{208}Pb(^{11}B, ^{10}Be)^{209}Bi reactions.

Orbit	E_x (MeV)	Allowed L	Present experiment Pot. 1 $\mathcal{S}_a\mathcal{S}_B$	Pot. 1 $\mathcal{S}_B$ [a]	Pot. 2 $\mathcal{S}_a\mathcal{S}_B$	Pot. 2 $\mathcal{S}_B$ [a]	Other experiments $\mathcal{S}_B(^3\text{He}, d)$ [b]	$\mathcal{S}_B(^{12}\text{C}, ^{11}\text{B})$ [c]	$\mathcal{S}_B(^{16}\text{O}, ^{15}\text{N})$ [d]	Theory $\mathcal{S}_B$ [e]	$u_{l_B j_B}^2$ ($r = 10$ fm) [f] (10^{-4} protons fm^{-3})
$3p_{3/2}$	3.12	0,1,2	0.25	0.58	0.32	0.74	0.58	0.84 ± 0.11	0.60 ± 0.05	0.74	1.4735
$2f_{5/2}$	2.82	2,3,4	0.15	0.35	0.20	0.47	0.61	0.60 ± 0.04	0.66 ± 0.09	0.66	0.8544
$2f_{7/2}$	0.90	2,3,4	0.22	0.51	0.29	0.67	0.65	0.64 ± 0.05	0.76 ± 0.06	0.85	0.6279
$1h_{9/2}$	0.0	4,5,6	0.20	0.47	0.30	0.70	0.54	0.74 ± 0.13	1.03 ± 0.03	0.95	0.2583
$1i_{13/2}$	1.61	5,6,7	0.26	0.60	0.35	0.81	0.52	0.51 ± 0.05	0.50	0.70	0.2030
$R_3 = f_{7/2}/f_{5/2}$			1.47		1.45		1.10	1.07 ± 0.11	1.15 ± 0.18	1.29	

[a] Assuming (Ref. 48) $\mathcal{S}_a = 0.43$.

[b] Reanalysis of data of Ref. 40, including nonlocality effects on distorted waves and finite range, using same proton wave function as in present analysis.

[c] From Ref. 14, using proton potential similar to ours except that $r_{so} = r_0$, $a_{so} = a$. Our potential 1 used for ^{11}B exit channel.

[d] From Ref. 13, using proton potential similar to ours except that $r_{so} = r_0$, $a_{so} = a$. Average over two energies. Assumes $\mathcal{S}_a = 2.0$ for $^{16}\text{O} = {}^{15}\text{N} + p$.

[e] From Ref. 40.

[f] Proton wave function using potential from Table II.

3). DWBA curves are included in Fig. 9, using either potential 1 (solid curves) or potential 2 (dashed curves) in both channels. The data are fitted quite well (except for the $1i_{13/2}$ group, where the cross sections are small). Again there is some preference for potential 2 which again gives peaks about 2° more forward than potential 1. In this case, however, the spectroscopic factors obtained with the two potentials differ by amounts between 30 and 50%. Over all, the values of S_B obtained (assuming[48] $S_a = 0.43$) are in fair agreement with, although generally larger than, those obtained from a consistent reanalysis of (^{3}He, d) data,[46] as shown in Table VII. However, it should be remembered that the values of S_a obtained from light-ion experiments (Table IV) are consistently larger than 0.43. This would lead to a reduction in the S_B from the present work and improve the agreement with the (^{3}He, d) analysis except for the $2f_{5/2}$ capture (and, to a lesser extent, the $2f_{7/2}$). Once again the ratio of spin-orbit partners, here R_3, is in disagreement with the light-ion results, at least for the choice of normalization of theory to experiment shown in Fig. 9.

Values of S_B obtained by Low and Tamura[13,14] from (^{12}C, ^{11}B) and (^{16}O, ^{15}N) data are also given in Table VII. They used proton bound states in ^{209}Bi similar to ours except for the spin-orbit term (they used $r_{so} = r_0$, $a_{so} = a$, which will lead to some j-dependent differences[28,46]). The agreement is good. The biggest deviations are for $2f_{5/2}$ and $1i_{13/2}$. At least part of the difference for $1i_{13/2}$ will be due to the different choice of bound-state spin-orbit term.[28,46] [It is also interesting to note that (^{12}C, ^{11}B) strips from a $1p_{3/2}$ orbit, which favors transfer into $j_B = l_B - \frac{1}{2}$, while (^{16}O, ^{15}N) strips from a $1p_{1/2}$ orbit, which favors the $j_B = l_B + \frac{1}{2}$ transfer.]

The deviations of the deduced S_B from unity are of the order expected theoretically. The predicted values from Ring and Werner[40] are included in Table VII; the results of Hamamoto[39] are in general agreement.

The spectrum in Fig. 6 shows groups corresponding to the ^{10}Be being emitted in its 3.37-MeV 2^+ state. The differential cross sections are shown in Fig. 10, together with DWBA calculations. The latter were made using the S_B values from Table VII and assuming[48] $S_a(1p_{3/2}) = 1.09$, $S_a(1p_{1/2}) = 0.05$ for $^{11}\mathrm{B} = {}^{10}\mathrm{Be}^* + p$. These calculations underestimate the cross sections for the $2f_{7/2}$ and $(2f_{5/2} + 3p_{3/2})$ groups and overestimate them for the $1i_{13/2}$ group. Uncertainties in the S_a values do not seem able to account for this. Simply scaling the S_a values scales all the predicted cross sections in the same way. Increasing the proportion of $1p_{1/2}$ component would enhance all the cross sections except that for $2f_{5/2}$. Consequently it seems there must be other reasons for the discrepancies such as contributions from multistep processes which would affect the transitions to the ground and excited states of ^{10}Be in different ways.

D. ^{208}Pb(^{11}B, ^{10}B)^{209}Pb reaction

In this case there is a serious mismatch between entrance and exit channels, $Q_{opt} = -2.2$, and the optimum transfer occurs with $L \approx 10$. Consequently the one-step transfers for small l_B are expected to be considerably inhibited and multistep or other processes may be important. Transfer to the $4s_{1/2}$ state in ^{209}Pb, which requires $L = 1$, would be particularly retarded and although there is a group close to the energy for this state (Fig. 4) we shall argue below that it is due to transfers to the $2g_{9/2}$ and $1j_{15/2}$ states associated with excited states of ^{10}B. Transitions to the $3d_{3/2}$ state at 2.54 MeV, if weak, could be hidden by the $2g_{7/2}$ group at 2.49 MeV. It is estimated that up to 10% of this peak might be due to $3d_{3/2}$ capture and this is approximately what is expected theoretically.

Figure 11 includes DWBA curves obtained using potential 1 in both channels. The spectroscopic factors used are given in Table VIII. The pre-

TABLE VIII. Spectroscopic factors for ^{208}Pb(^{11}B, ^{10}B)^{207}Pb reaction.

Orbit	$4s_{1/2}$	$3d_{5/2}$	$2g_{9/2}$	$2g_{7/2}$	$1i_{11/2}$	$1j_{15/2}$
E_x (MeV)	2.03	1.57	0.0	2.49	0.78	1.42
Allowed L	1	1, 2, 3	3, 4, 5	3, 4, 5	5, 6, 7	6, 7, 8
$S_a S_B$ [a]	1.07	1.07	1.5	1.7	1.7	0.64
S_B [b]	0.98 [c]	0.98 [c]	1.38	1.56	1.56	0.58 [c]
$u_{l_B j_B}^2(r = 10\ \mathrm{fm})$ [d]	9.260	6.333	2.294	2.883	0.3866	0.6478

[a] Correspond to curves shown in Figs. 12 and 13.
[b] Assuming (Ref. 48) $S_a = 1.09$.
[c] From (d,p) measurements of Ref. 47.
[d] Neutron wave functions using potential from Table II, in 10^{-4} neutrons fm^{-3}.

dicted angular distributions are shifted in angle appreciably compared to the experimental ones. The values of $\mathcal{S}_B$ required for the $2g$ and $1i_{11/2}$ states are excessive (unless the assumed[48] value of $\mathcal{S}_a = 1.09$ is incorrect). We did not make an extensive study of the effects of using other optical potentials, but use of potential 2 in both channels has rather little effect; in particular, it does not move the cross section peaks into agreement with the data as happened with the other reactions.

The $1j_{15/2}$ and $3d_{5/2}$ groups could not be properly resolved; their summed strength is shown in Fig. 11. The theoretical curve uses $\mathcal{S}_B$ values from a recent (d, p) measurement.[47] The predicted magnitude is close to the observed one, but again the data peak further forward. Experimentally we estimate the $j_{15/2}$ contribution to be between 2 and 4 times the $d_{5/2}$ contribution, and theoretically the ratio predicted (using the $\mathcal{S}_B$ of Table VIII) varies from 2 at $\theta = 55$ and 75° to 4.4 at 60°.

The group corresponding to an apparent excitation in ^{209}Pb of about 2.1 MeV could be due to $2g_{9/2}$ transfer with ^{10}B* in its excited 2.15-MeV 1^+ state and $1j_{15/2}$ transfer with ^{10}B* in its 0.717-MeV 1^+ state, as well as the $4s_{1/2}$ transfer with ^{10}B unexcited. Figure 12 shows the data and the corresponding DWBA calculations. The predicted $4s_{1/2}$ cross section, assuming[48] $\mathcal{S}_a = 1.09$ and taking $\mathcal{S}_B = 0.98$ from the (d, p) measurement,[47] is about 30 times too small and peaks at the wrong angle. (If the Q value were -5 MeV instead of -9.55 MeV, the peak would be at about 60° with a value of about 1 mb/sr, larger than the data. If $Q = 0$, the peak cross section increases by another factor of 60 and moves in to 55°.)

For the excited ^{10}B we took the CK predictions[48] of $\mathcal{S}_a(1p_{3/2})$ and $\mathcal{S}_a(1p_{1/2})$ (both are allowed for both excited states), with the $\mathcal{S}_B$ from the (d, p) measurement.[47] The sum is calculated to be appreciably larger than the observed cross sections and peaks at too large angles just like the distributions for the other states. Of course the magnitude is uncertain because the $\mathcal{S}_a$ are uncertain, but it is reasonable to suppose that this explanation of the 2.1-MeV group is basically correct.

Other excited ^{10}B* groups might be contributing to the states displayed in Fig. 11. The 0.717-MeV state of ^{10}B associated with $2g_{9/2}$ capture could contribute to the $1i_{11/2}$ ($E_x = 0.78$ MeV) group, while when associated with $1i_{11/2}$ capture it has a Q value similar to the $3d_{5/2} + 1j_{15/2}$ transfers. Again, the 1.74-MeV state of ^{10}B accompanying $1i_{11/2}$ capture would appear close to the $2g_{7/2} + 3d_{3/2}$ groups. These coincidences could be partly responsible for the large $\mathcal{S}_B$ values deduced for these states; however, such an explanation is *not* available for the $2g_{9/2}$ ground state transfer.

E. Bound-state form factor values

As remarked earlier, the separation into bound-state wave function and spectroscopic factor is a theoretical artifact. What enters the transition amplitude (3) are overlaps of wave functions for n- and $(n+1)$-nucleon systems, integrated over the coordinates of all but the extra nucleon. The result is a "form factor,"[37] whose radial part is $R_{lj}(r)$, and the transfer reaction measures the magnitude of this at some large value of r near the strong absorption radius. In the DWBA calculations we use the single-particle model for the form factor

$$R_{lj}(r) \approx \zeta_{lj} u_{nlj}(r) , \tag{9}$$

where $u_{nlj}(r)$ is an eigenfunction for the (nlj) orbit in a Woods-Saxon potential, normalized so that

$$\int u_{nlj}^2(r) r^2 dr = 1.$$

The corresponding spectroscopic factor is $\mathcal{S} = \zeta_{lj}^2$. However, we may avoid all the ambiguities of choice of potential well for $u_{nlj}(r)$ (Sec. VII B above) by quoting values of $R_{lj}(r)$ directly. The shape of the tail of $R_{lj}(r)$ is determined by the separation energy and this is reproduced correctly by the model (9). Further, the cross sections for the present experiment are simply proportional to the square of the tails of the $R_{lj}(r)$ for the ^{208}Pb ± 1 system if the post interaction is used. Hence we may extract from the data values for the $R_{lj}(r)$ at some large radius which are independent of the model (9) which is used. This technique has been used previously for light-ion measurements.[28,33] (Of course uncertainties, such as those due to optical potentials and interaction terms, still remain.)

Rather than introduce another large table, we include in Tables V–VIII values of u_{nlj}^2 ($r = 10$ fm) for the wave functions used in the analyses. The interested reader then may use Eq. (9) and the quoted $\mathcal{S}_B$ values to deduce R_{lj}^2 ($r = 10$ fm). We chose $r = 10$ fm because the largest contributions to the transfers in the present experiment occur for $r_{xA} \approx 10$ fm. The wave functions have essentially reached their asymptotic form at 10 fm.

VIII. SUMMARY

Differential cross sections were obtained for all four possible single-nucleon transfers induced by 72.2-MeV ^{11}B ions on ^{208}Pb, exciting single-particle or single-hole states in the residual nucleus. Some groups corresponding to the light ion being left in an excited state were also identified. The angular distributions all display the single broad

peak expected from the classical Rutherford orbit for grazing collisions.

The application of the DWBA of these reactions was discussed in some detail, particular attention being paid to various uncertainties. The major uncertainties arise from the choice of optical potentials (especially in the exit channels) and of the form factors for the bound nucleon before and after transfer.

Except for the (^{11}B, ^{10}B) reactions which suffer an unfavorable matching between incoming and outgoing orbits, the predicted angular distributions are in good agreement with the data, and the spectroscopic factors extracted are generally close to the values expected and to the values obtained in other light- and heavy-ion experiments. The over-all success argues strongly in favor of the interpretation of these reactions as predominantly one-step processes which can be described by the DWBA to a good approximation when there is good matching between entrance and exit channels. When the matching is poor, as in the case for (^{11}B, ^{10}B), clearly other effects have to be taken into account. There is also some evidence of the need for other effects from the data for emission of the light ion in an excited state.

APPENDIX

An important step in the calculation of the amplitude (3) is to evaluate numerically the multipole integrals which, in the post form, are given by

$$g_K(r_{aA}, r_{bB}) = \int_{-1}^{1} d\mu\, P_K(\mu) u_B(r_{xA}) u_a(r_{xb}) V_{bx}(r_{xb}), \tag{A1}$$

where $\mu = \cos\theta$ and θ is the angle between $\vec{r}_{aA}$ and $\vec{r}_{bB}$ (see Fig. 16). Also u_B, u_a are the radial form factors for the particle x bound in B and a, respectively, while V_{bx} is the b-x binding potential. The number of K values required is a few more than the number of partial waves to be used, and the integral (A1) is to be done for every pair of values r_{aA} and r_{bB}. The evaluation of the g_K was by far the most time-consuming part of the calculation with the original finite-range code[60] FANNY. The code LOLA used here makes use of the Gauss-Legendre integration method, already an improvement. When the full range $0 \leq \theta \leq 180°$ was used, a high order of Gauss-Legendre integration was required, of the order of 4 times K_{max}, before an accurate result was obtained. (We aim for an accuracy of $\lesssim 1\%$ in the cross section.) However, in many cases the integrand in (A1) is strongly concentrated near $\mu = 1$ or $\theta = 0$. For example, in (^{11}B, ^{10}Be), when the nuclei are separated by the strong absorption radius of about 12.2 fm, the integrand of (A1) peaks strongly for $r_{xb} \approx 2.3$ fm, $r_{xA} \approx 9.9$ fm, with a width of about 2 fm, when x is on the line joining the centers of the two core nuclei (i.e., $\mu = 1$ or $\theta = 0$). When x moves off this line, the integrand decreases rapidly mainly because r_{xb} increases and the product $u_a V_{bx}$ has a short range; for $\theta = 1°$, x has moved off about 2 fm and the integrand has decreased by a factor of 5; for $\theta = 2°$ these become 4 fm and a factor of 10^3, respectively. (However, it is these off-line $\theta \neq 0$ contributions which allow the nonnormal parity transfers.)

For ^{11}B + ^{208}Pb we found that $\theta < 2$ or 3° was adequate, although the calculations reported here used $\theta_{max} = 5°$. This allows a very low order of integration to be used (we used an order of 20) even for large K and such an increase in speed that now the g_K evaluation takes only a small fraction of the total time.

The remainder of the calculation involves radial integrals of the form

$$\int dr_{aA} \int dr_{bB}\, \chi_{L_b}(r_{bB})\, F_{lL_aL_b}(r_{aA}, r_{bB})\, \chi_{L_a}(r_{aA}), \tag{A2}$$

where the χ_{L_i} are partial distorted waves for the entrance and exit channels and the $F_{lL_aL_b}$ are sums of the g_K weighted by angular momentum coefficients. Examination of the form factors F shows them in many cases to be concentrated along the diagonal $r_{aA} \approx r_{bB}$. For ^{11}B + ^{208}Pb at 72 MeV we find this band to be only $\lesssim 1$ fm wide; very good accuracy was obtained by restricting the integration to a band of width 2 fm.

The wave numbers involved in the χ are generally large ($k \approx 6$ fm^{-1} for ^{11}B + ^{208}Pb at 72 MeV) and this would seem to require very small (and hence very many) steps in r_{aA} and r_{bB}. Fortunately this is not the case for well-matched grazing collisions. In the cases here, a step length of 0.1 fm

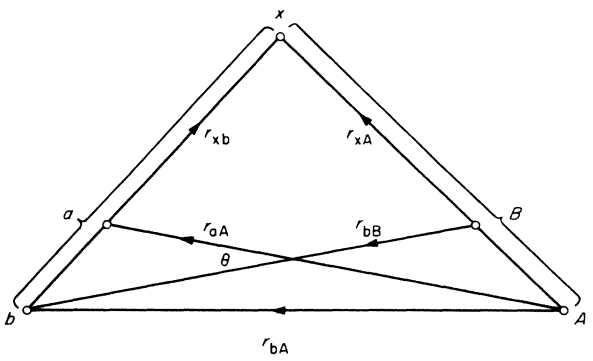

FIG. 16. Vector diagram relating the position vectors which are involved in the DWBA amplitude.

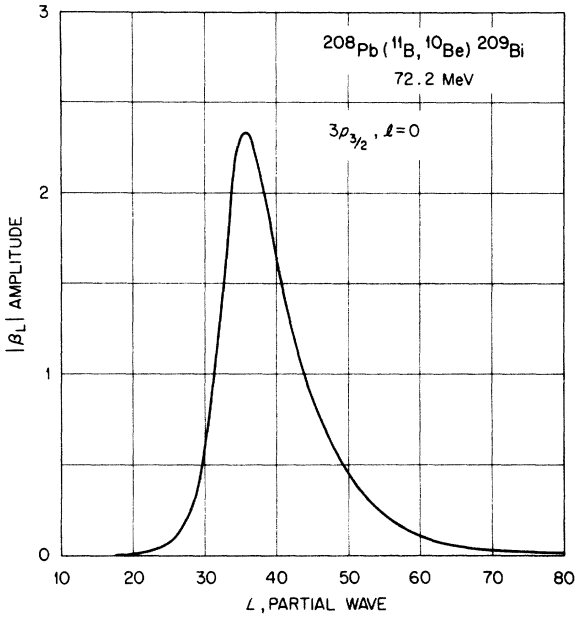

FIG. 17. Distribution of the partial wave amplitudes against angular momentum for a typical single-nucleon transfer.

across the ridge in $F_{lL_aL_b}$ gave good accuracy with Simpson's rule; the remaining integration could then use steps 2 or 3 times larger without loss of accuracy. [More care was necessary with the poorly matched (^{11}B, ^{10}B) reactions; smaller step lengths and a larger range of radii and partial waves was required for these.]

The strong absorption associated with heavy ions allows a further economy. Contributions from radii less than some minimum value (~ the target nucleus radius) and from partial waves with L_i less than the corresponding angular momentum are negligible. The distribution of reaction amplitudes with respect to $L_a = L_b$ for $L = 0$ transfer in a (^{11}B, ^{10}Be) reaction is shown in Fig. 17. Other reactions and other L transfers show the same behavior. The peak corresponds to the grazing collision orbit. For the calculations reported here we used $R_{\min} = 8$ fm, $L_{\min} = 20$, except for (^{11}B, ^{10}B) where $R_{\min} = L_{\min} = 0$. Figure 17 also shows that an $L_{\max} = 80$ is adequate; we used $R_{\max} = 20$, which is the distance of closest approach of the corresponding classical Rutherford orbit.

Very roughly, the computing time on the IBM-360/91 for the ORNL version of LOLA is

$$\tau \approx (\mathrm{NRA})(\mathrm{NRB})[(\mathrm{NG})(\mathrm{NK})\mathring{\tau}_{\mathrm{GK}} + \mathrm{NL}(L+1)(2l_a+1)(2l_B+1)\mathring{\tau}_L],$$

where NRA, NRB are the number of radial steps in the r_{aA}, r_{bB} directions; NG is the order of the Gauss-Legendre integration for Eq. (A1), NK is the number of K values required, NL is the number of partial waves to be used and L is the L transfer. Then $\mathring{\tau}_{\mathrm{GK}} \approx 3\times10^{-6}$ sec, $\mathring{\tau}_L \approx 2\times10^{-5}$ sec.

The code was tested in a number of ways. For example, replacing the distorted waves in the amplitude (3) by plane waves allows one to obtain semianalytic expressions, proportional to the Fourier transforms of u_B and $V_{bx}u_a$. The code reproduced these to a high degree of accuracy. A comparison was also made with some calculations by the independent code SATURN-MARS [13,14] and satisfactory agreement obtained. (We are indebted to T. Tamura for sending us these.)

---

*Research sponsored by the U. S. Atomic Energy Commission under contract with Union Carbide Corporation.

†Present address: Nuclear Structure Laboratory, University of Rochester, Rochester, New York 14627.

‡Research participation at Oak Ridge National Laboratory supported in part by Oak Ridge Associated Universities.

[1]J. S. Larsen, J. L. C. Ford, Jr., R. M. Gaedke, K. S. Toth, J. B. Ball, and R. L. Hahn, Phys. Lett. 92B, 205 (1972).

[2]J. L. C. Ford, Jr., K. S. Toth, D. C. Hensley, R. M. Gaedke, P. J. Riley, and S. T. Thornton, Argonne National Laboratory Report No. PHY-1973B (unpublished), Vol. II.

[3]N. Anyas-Weiss, J. Becker, T. A. Belote, J. C. Cornell, P. S. Fisher, P. H. Hudson, A. Menchaca-Rocha, A. D. Panagiotou, and D. K. Scott, Phys. Lett. 45B, 231 (1973).

[4]D. G. Kovar, B. G. Harvey, F. D. Becchetti, J. Mahoney, D. L. Hendrie, H. Homeyer, W. von Oertzen, and M. A. Nagarajan, Phys. Rev. Lett. 30, 1075 (1973); D. G. Kovar, F. D. Becchetti, B. G. Harvey, F. Pülhoffer, J. Mahoney, D. W. Miller, and M. S. Zisman, Phys. Rev. Lett. 29, 1023 (1972).

[5]F. Pougheon and P. Roussel, Phys. Rev. Lett. 30, 1223 (1973).

[6]H. J. Körner, G. C. Morrison, L. R. Greenwood, and R. H. Siemssen, Phys. Rev. C 7, 104 (1973).

[7]T. J. Lewis, G. H. Wedberg, J. C. Peng, J. L. Ricci, C. M. Cheng, and J. V. Maher, Phys. Rev. C 8, 678 (1973).

[8]D. K. Scott, P. N. Hudson, P. S. Fisher, C. U. Cardinal, N. Anyas-Weiss, A. D. Panagiotou, and P. J. Ellis, Phys. Rev. Lett. 28, 1659 (1972).

[9]M. S. Zisman, F. D. Becchetti, B. G. Harvey, D. G. Kovar, J. Mahoney, and J. D. Sherman, Phys. Rev. C 8, 1866 (1973).

[10]S. Landowne, R. A. Broglia, and R. Liotta, Phys. Lett. 43B, 160 (1973); N. K. Glendenning and R. J. Ascuitto, *ibid.* 45B, 85 (1973); K. S. Low and T. Tamura, in Argonne National Laboratory Report No.

PHY-1973B (unpublished), Vol. II.
[11]R. M. Gaedke, K. S. Toth, and I. R. Williams, Phys. Rev. 141, 996 (1966).
[12]R. M. DeVries and K. I. Kubo, Phys. Rev. Lett. 30, 325 (1973); R. M. DeVries, Phys. Rev. C 8, 951 (1973); J. L. Perrenod and R. M. DeVries, Phys. Lett. 36B, 18 (1971).
[13]T. Tamura and K. S. Low, Phys. Rev. Lett. 31, 1356 (1973).
[14]K. S. Low and T. Tamura, Phys. Lett. 48B, 285 (1974).
[15]J. L. C. Ford, Jr., P. H. Stelson, and R. L. Robinson, Nucl. Instrum. Methods 98, 199 (1972).
[16]B. G. Harvey, J. Mahoney, F. G. Pülhoffer, F. S. Goulding, D. A. Landis, J. C. Favire, D. G. Kovar, M. S. Zisman, J. R. Meriwether, S. W. Casper, and D. L. Hendrie, Nucl. Instrum. Methods 104, 21 (1972).
[17]C. J. Borkowski and M. K. Kopp, Rev. Sci. Instrum. 39, No. 10, 1515 (1968).
[18]C. J. Borkowski and M. K. Kopp, IEEE Trans. Nucl. Sci. NS-17, No. 3, 340 (1970).
[19]M. R. Schmorak, R. L. Auble, M. B. Lewis, and M. J. Martin, Nucl. Data B5, 205 (1971).
[20]P. J. A. Buttle and L. J. B. Goldfarb, Nucl. Phys. A176, 299 (1971).
[21]R. A. Broglia and A. Winther, Nucl. Phys. A182, 112 (1972).
[22]D. M. Brink, Phys. Lett. 40B, 37 (1972).
[23]F. G. Perey, unpublished; modified by C. Y. Wong and L. W. Owen to include up to 500 partial waves.
[24]F. D. Becchetti, D. G. Kovar, G. B. Harvey, J. Mahoney, B. Mayer, and P. G. Pühlhover, Phys. Rev. C 6, 2215 (1972).
[25]J. L. C. Ford, K. S. Toth, D. C. Hensley, R. M. Gaedke, P. J. Riley, and S. T. Thornton, Phys. Rev. C 8, 1912 (1973).
[26]R. da Silveira, in *Proceedings of the International Conference on Nuclear Physics, Munich, 1973,* edited by J. de Boer and H. J. Mang (North-Holland, Amsterdam/American Elsevier, New York, 1973), Contribution No. 5.40.
[27]N. Austern, *Direct Nuclear Reaction Theories* (Wiley-Interscience, New York, 1970).
[28]W. C. Parkinson, D. L. Hendrie, H. H. Duhm, J. Mahoney, J. Saudinos, and G. R. Satchler, Phys. Rev. 178, 1976 (1969).
[29]See, for example, G. R. Satchler, Argonne National Laboratory Report No. PHY-1973B (unpublished), Vol. I, and other references given there.
[30]P. J. A. Buttle and L. J. B. Goldfarb, Nucl. Phys. A176, 299 (1971).
[31]C. J. Batty and G. W. Greenlees, Nucl. Phys. A133, 673 (1969).
[32]M. Dost, W. R. Hering, and W. R. Smith, Nucl. Phys. A93, 357 (1967).
[33]H. J. Korner and J. P. Schiffer, Phys. Rev. Lett. 27, 1457 (1971).
[34]J. W. Negele, Phys. Rev. C 1, 1260 (1970); 9, 1054 (1974).
[35]D. H. Wilkinson and M. E. Mafethe, Nucl. Phys. 85, 97 (1966).
[36]G. Fey, H. Frank, W. Schultz, and H. Thiessen, Z. Phys. 265, 401 (1973).
[37]G. M. McAllen, W. T. Pinkston, and G. R. Satchler, Particles and Nuclei 1, 412 (1971).
[38]B. A. Watson, P. P. Singh, and R. E. Segel, Phys. Rev. 182, 977 (1969).
[39]I. Hamamoto, Nucl. Phys. A141, 1 (1970).
[40]P. Ring and E. Werner, Nucl. Phys. A211, 198 (1973).
[41]D. Royer, M. Arditi, L. Bimbot, H. Doubre, N. Frascaria, J. P. Garron, and M. Riou, Nucl. Phys. A158, 516 (1970).
[42]C. A. Whitten, N. Stein, G. E. Holland, and D. A. Bromley, Phys. Rev. 188, 1941 (1969); G. R. Satchler, Phys. Rev. C 4, 1485 (1971).
[43]S. M. Smith, P. G. Roos, C. Moazed, and A. M. Bernstein, Nucl. Phys. A173, 32 (1971).
[44]W. A. Lanford and G. M. Crawley, Phys. Rev. C 9, 646 (1974).
[45]G. J. Igo, P. D. Barnes, E. R. Flynn, and D. D. Armstrong, Phys. Rev. 177, 1831 (1969).
[46]B. H. Wildenthal, B. M. Preedom, E. Newman, and M. R. Cates, Phys. Rev. Lett. 19, 960 (1967).
[47]D. G. Kovar, N. Stein, and C. K. Bockelman, unpublished.
[48]S. Cohen and D. Kurath, Nucl. Phys. A101, 1 (1967).
[49]W. Fitz, R. Jahr, and R. Santo, Nucl. Phys. A101, 449 (1967).
[50]D. Miljanic, M. Furic, and V. Valkovic, Nucl. Phys. A119, 379 (1968).
[51]D. Miljanic and V. Valkovic, Nucl. Phys. A176, 110 (1971).
[52]J. E. Monahan, H. T. Fortune, C. M. Vincent, and R. E. Segel, Phys. Rev. C 3, 2192 (1971).
[53]G. S. Mutchler, D. Rendic, D. E. Velkley, W. E. Sweeney, and G. C. Phillips, Nucl. Phys. A172, 469 (1971).
[54]F. Hintenberger, G. Mairle, U. Schmidt-Rohr, P. Turek, and G. J. Wagner, Nucl. Phys. A106, 161 (1968).
[55]G. M. Reynolds, D. E. Rundqvist, and R. M. Poichar, Phys. Rev. C 3, 442 (1971).
[56]P. D. Miller, J. L. Duggan, M. M. Duncan, R. L. Dangle, W. R. Coker, and J. Lin, Nucl. Phys. A136, 229 (1969).
[57]R. M. DeVries, G. R. Satchler, and J. G. Cramer, Phys. Rev. Lett. 32, 1377 (1974).
[58]W. Tobocman, R. Ryan, A. J. Baltz, and S. H. Kahana, Nucl. Phys. A205, 193 (1973).
[59]D. F. Jackson and R. C. Johnson, Phys. Lett. 49B, 249 (1974); R. C. Johnson and P. J. R. Soper, Nucl. Phys. A182, 639 (1972).
[60]R. M. Drisko, unpublished; R. M. Drisko and G. R. Satchler, Phys. Lett. 9, 342 (1964).